AN ABSTRACT OF THE THESIS OF

Maha D. Alghamdi for the degree of Master of Science in Chemistry presented on June 13, 2014

Title: Theoretical Study of Beryllium Borohydride $Be(BH_4)_2$

Abstract approved: _____

Joseph W. Nibler Wei Kong

Ab initio calculations using the B3LYP and CCSD(T) methods were employed in this work to explore the most stable structure of the intriguing compound $Be(BH_4)_2$, for which as many as seven different structures have been proposed in the literature. Use of the B3LYP density functional method with several large basis sets predicts the classic D_{2d} structure to be the lowest energy form, but with a D_{3d} configuration having an energy minimum only 353 cm^{-1} higher in energy. Potential energy surfaces were calculated using BH_4 torsional and tumbling coordinates and these showed a low energy barrier of 553 cm^{-1} for interconversion of the two forms. Similar calculations were done using the CCSD(T) method, which is usually considered the "gold standard" of quantum calculations. These were much more time intensive and gave the reverse ordering, with the D_{3d} configuration 90 cm^{-1} lower in energy than the D_{2d} form. In all cases, inclusion of zero point energy calculated for both isomers tended to lower the ground state energy of the D_{3d} structure relative to that of the D_{2d} form. It is concluded that the D_{3d} structure is the most stable form of $Be(BH_4)_2$ but that a substantial fraction of the molecules exist in the D_{2d} form in the room temperature vapor.

Recent versions of the Gaussian program used in this work allow calculations of

anharmonic properties of a molecule and these were done to predict more accurate vibration-rotation parameters as well as infrared and Raman intensities. These were employed in a reexamination of several earlier experimental infrared spectra. Comparison of the predicted and experimental spectra of $Be(BH_4)_2$ vapor shows the clear presence of both forms in the room temperature vapor. When $Be(BH_4)_2$ is isolated in an argon matrix at 20 K, only infrared features attributable to the D_{3d} form remain, a result consistent with the predictions of the CCSD(T) calculations.

Previous infrared spectra of the vapor at 0.0015 cm^{-1} resolution showed no resolvable vibration-rotation transitions, but concurrent studies in a cold jet revealed many sharp lines with width comparable to the resolution. The jet spectra were quite limited in range however, and efforts to simulate these using theoretical vibration-rotation parameters were unsuccessful. Possible reasons for the extreme congestion of features in both the jet and room temperature spectra are discussed.

Theoretical Study of Beryllium Borohydride $Be(BH_4)_2$

by

Maha D. Alghamdi

A THESIS

Submitted to

Oregon State University

in partial fulfillment of
the requirements for the
degree of

Master of Science

Presented June 13, 2014

Commencement June 2014

Master of Science thesis of Maha D. Alghamdi presented in June 13, 2014

Approved:

Co-Major Professor, representing Chemistry

Co-Major Professor, representing Chemistry

Chair of the Department of Chemistry

Dean of the Graduate School

I understand that my thesis will become part of the permanent collection of Oregon State University libraries. My signature below authorizes release of my thesis to any reader upon request.

Maha D. Alghamdi, Author

ACKNOWLEDGEMENTS

Thank you god for turning my dreams true and taking my hand to overcome the obstacles I faced. Special thanks to my family. Words cannot express how grateful I am to my parents, who did everything to raise the love of knowledge in me and were one of the reasons to facilitate my journey to the graduate degree. Your prayer for me was what sustained me thus far and I will always count on you. Thank you my siblings for believing in me and motivating me to achieve my goals. I am lucky to have you in my life.

I am deeply thankful to my caring, loving, and supportive husband, Hussain, who took me in this long journey to pursue my dreams with no expectations or demands and always was such an encouraging and joyful person. My heartfelt appreciation for your patience, flexibility and understanding along this journey.

My sincere gratitude for my two advisors, Dr. Joseph Nibler and Dr. Wei Kong. Dr. Nibler, I am thankful for all the time you spent helping and educating me. You have been a tremendous mentor for me who I learned a lot from in many aspects. Your excellent guidance, patience, motivation, enthusiasm, and wide knowledge made theoretical chemistry very interesting to me. Dr. Wei, thank you for you amazing personality and very helpful discussions and suggestions. Your group meetings were very informative and helpful.

Last but not the least, I would also like to thank all of my friends who supported me in writing and were very interested to hear about my project and provided me with several great ideas.

CONTRIBUTION OF AUTHORS

This research was carried out with the guidance and supervision of Dr. Joseph Nibler. This work utilizes advances in computers and in software to extend some previous theoretical calculations on this molecule done at OSU as part of the PhD thesis research of Abdullah Al-Kahtani (1995) and Darren Williams (1997). All experimental spectra are from the literature or from infrared spectra obtained at room temperature or in a jet by these two students

TABLE OF CONTENTS

Page

TABLE OF CONTENTS (CONTINUED)

Page

LIST OF FIGURES

Figure Page

LIST OF TABLES

Table Page

Theoretical Study of Beryllium Borohydride $Be(BH_4)_2$

Chapter I. Summary of Previous Experimental and Theoretical Work

Introduction

Few classes of compounds show as much variety in their bonding characteristics as the metal borohydrides, with bonding characterized as mainly ionic in the alkali metal borohydride salts but covalent in volatile compounds such as $Al(BH_4)_3$ and $Zr(BH_4)_4$. Included in the latter category is beryllium borohydride, one of the most puzzling of the metal borohydrides. Since its synthesis in 1940, much effort has been employed to resolve the structure of this intriguing compound. A survey of the seventy-four year history of $Be(BH_4)_2$ reveals an array of different and even contradictory results, some of which are detailed here.

Experimental Studies

Beryllium borohydride was first synthesized in 1940 by Burg and Schlesinger, by adding diborane to dimethylberyllium and treating the product with diborane until beryllium borohydride was obtained as the main product.[1] These authors suggested that the molecule is monomeric in the gas phase but polymeric in the solid phase. The polymeric nature of the solid was established by a subsequent x-ray diffraction experiment[2] and by an infrared vibrational study[3]. The polymer was found to consist of coupled $BeBH_4^+$--BH_4^- ions linked via double hydrogen bridges, an arrangement that was in agreement with a theoretical calculation by Marynick in 1979.[4] The only other investigation of a solid form of $Be(BH_4)_2$ was a recent x-ray diffraction experiment of a carbene complex in 2012, [5] in which double hydrogen bridges were also seen.

On the other hand, the structure of the gas phase monomeric form of $Be(BH_4)_2$ has been more controversial. Some of the structures considered for this molecule are shown in

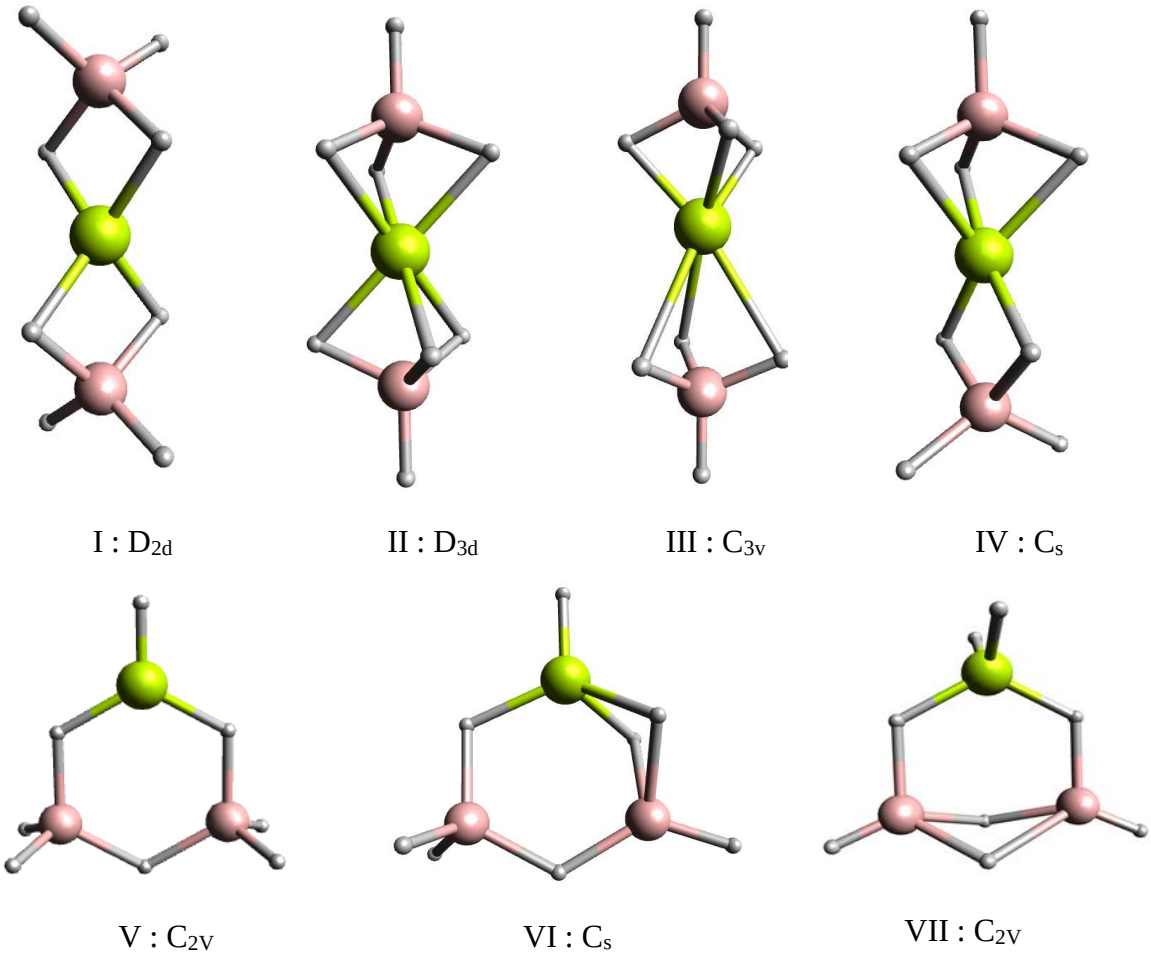

Figure 1.1: Structures that have been proposed for $Be(BH_4)_2$

Figure1.1. The first structure proposed was a D_{2d} form (fig. 1.1 I), based on an infrared study by Longuet-Higgens and Bell in 1943.[6] This was disputed by Silibiger and Bauer from an electron diffraction analysis done in 1946 which was said to favor a D_{3d} structure (fig. 1.1 II).[7] However later that same year, the electron diffraction data was reinterpreted and said to support a D_{2d} structure, with the bridging hydrogens closer to B than Be. Thus this double-bridged form was accepted and presented as an interesting example of hydrogen bridge-bonding in most inorganic textbooks.

The picture changed in 1967 when Almenningen, Gundersen and Haaland did another electron diffraction investigation and proposed a totally different structure, a triangular, polar

form with C_{2v} symmetry, (fig. 1.1 VII)[8]. This controversial result stimulated several research endeavors to reveal the correct structure. In 1970, Morgan and Cook obtained higher resolution infrared spectra of the vapor and suggested that the vibration-rotation contours they observed were most consistent with a triangular C_{2v} structure, but with double hydrogen bridges between the heavy atoms and with no terminal BeH bonds[9] (not shown in the figure). In the same period, Nibler and colleagues did electric deflection[10] and dielectric[11] measurements that indicated that $Be(BH_4)_2$ was polar, with a dipole moment value of about 2 Debye. From infrared studies of $Be(BH_4)_2$ in the vapor and in argon matrices, Nibler concluded that the vapor must consist of two stable forms of $Be(BH_4)_2$ at room temperature.[12] The vapor spectra were consistent with D_{2d} and D_{3d} forms, with the former the higher energy form since features attributable to it were absent in the low temperature matrix spectra. To account for the polar nature of the molecule, he proposed that the lowest energy form of $Be(BH_4)_2$ might have the Be atom off center, yielding a polar C_{3v} structure, fig. 1.1 III.

The variety of forms proposed encouraged more examination. Gundersen et al.[13] repeated the electron diffraction measurement in 1973, obtaining results different from any of the earlier electron diffraction studies. They suggested a linear structure, with D_{3d} symmetry (fig. 1.1 II). The inconsistency of the electron diffraction results was subsequently explored in another experiment by Haaland, Nova and Bredhaugen.[14] They found that the time after the sample-preparation affected the electron diffraction pattern. They suggested that this could be due to a non-equilibrium distribution of forms, or could be a result of sample decomposition. Evidence for the latter was also seen in the infrared studies[15], which showed that the sample undergoes reaction with salt windows and decomposes slowly on metal surfaces. This observation brought into question the dipole moment deduced from the dielectric measurements, since these were made in a capacitance cell with metal electrodes. However, the electric deflection results, coupled with concurrent mass spectral measurements, seemed to

clearly show the presence of a polar form of $Be(BH_4)_2$ in the molecular beam. Several later efforts to obtain microwave spectra of $Be(BH_4)_2$ proved unsuccessful, either due to absence of a dipole moment or to sample decomposition in metal waveguides.

An investigation of the vapor was published in 1977. It claimed with certainty a linear framework of Beryllium Borohydride but without distinction between the linear forms.[16] All hydrogens were found to be equivalent on the NMR time scale because of the rapid interchange of the hydrogens due to the high fluxionality of $Be(BH_4)_2$. Similar conclusions were reached by Al-Kahtani in an NMR investigation done as part of his PhD thesis[17].

Theoretical Studies

Theoretical investigations of the structure of $Be(BH_4)_2$ were stimulated by the controversial experimental results. The first theoretical study was done in 1968,[18] to see if theory would support the triangular BBeB arrangement that had been suggested by the electron diffraction results of Almenningeng et. al. in 1967. Ab initio calculations were done using a basis set of 34 Gaussian-type atomic orbitals (G.T.O's). It was found that D_{2d} form had the lowest energy but the authors suggested that further calculations with changed bond lengths and angles of a triangular structure might be worthwhile. In 1973, Marynik and Lipsomb did calculations for many possible structures, using HF-SCF and CI (CISD) methods.[19] They concluded that the calculation supported three possible stable structures (fig. 1.1 I, II and IV), with the D_{2d} (I) structure the most stable form followed by IV and then II (relative energies of 0, 31 and 27 KJ mol^{-1} respectively). Structures V and VII were considered unlikely to occur, the former C_{3v} structure reverting to a D_{3d} form during optimization whereas the latter triangular arrangement was much higher in energy compared to the lowest energy D_{2d} form.

Ahlrichs, in 1973,[20] did another theoretical exploration where he used Gaussian functions with an independent electron pair approximation to account for correlation. The D_{2d}

structure had lower energy without correlation, but with it, the D_{3d} form was found to be more stable. In 1986, the same trend was observed using many body perturbation theory (MBPT) calculation.[21] Three years later, Stanton and Lipsomb used MBPT(4) calculations with a basis set of 85 contracted Gaussian functions and found that both D_{2d} and D_{3d} structures (fig. 1.1 I and II) were stable forms of $Be(BH_4)_2$.[22] The D_{2d} structure was found to be slightly lower in energy but the uncertainty in the results made this conclusion tentative. Stanton argued against the existence of a C_{3v} symmetry structure that had been proposed to account for the dipole moment evidence. In 1990, Banarsi performed theoretical treatment using different levels of calculations.[23] The D_{2d} structure had lower energy in the SCF and MP4 levels while the D_{3d} form was lower on the MP2 level. Both structures had the same energy on the MP3 level.

In 1994, ab initio calculations were done using density function theory (DFT).[24] The best quality calculations in this study were judged to be MP4/6-311G and MP2/6-311G which both found the D_{3d} structure to be lower in energy. Stanton revisited $Be(BH_4)_2$ in 1996, trying to find some structure that would explain the reported dipole moment.[25] He found a new polar, triangular structure (Fig. 1.1 V1) to be a stationary point on the potential energy surface. However, the energy of this point was about 80 kJ mol^{-1} above the energy of the linear D_{2d} and D_{3d} forms, indicating that only a small amount of the polar structure would be present in the room temperature equilibrium mixture.

Most Recent Studies

In 1996, Darren Williams, as part of his phD dissertation [26], did some additional theoretical calculations, along with some new, higher resolution FTIR measurements on gaseous $Be(BH_4)_2$. The ab initio calculations employed the MP2 method with a 6-311G** basis set, which predicted a D_{3d} structure as the lowest energy form, with the D_{2d} form slightly higher.

The infrared spectra, even at 0.0015 cm^{-1} resolution, showed only broad bands in the vapor, with no hint of distinct vibration-rotation transitions. One possible cause of this could be line broadening caused by a short lifetime of any state due to rapid interconversion from one structural form to another. A second possibility could simply be extreme congestion due to various structures, each with ^{11}B and ^{10}B variants and with hot bands due to thermal population of low-lying vibrational states.

In an effort to reduce thermal effects, Williams used the molecular beam diode laser apparatus of Dr. Steve Sharpe of the Pacific Northwest National Laboratory to obtain an infrared spectrum of $Be(BH_4)_2$ cooled to 10 to 20K by expansion in an argon jet. The resultant spectrum showed clear, sharp vibration-rotation features, eliminating lifetime broadening as the cause of the unresolved room temperature spectra.[26] Due to the small amount of sample, only a very limited range (2164-2167 cm^{-1} and 2193- 2197 cm^{-1}) was examined and efforts to simulate the spectra and make assignments of the individual vibration-rotation transitions were inconclusive.

This Study

Computational chemistry is getting more powerful and more reliable. This development is due largely to the huge improvement in the speed of personal computers but also to improvements to electronic structure programs. For example, a UMP2/6-311G** calculation that William carried out in 1996 took about three hours but now can be done in less than a minute. The Gaussian 09 versions that are widely used for quantum electronic structure calculations now permit computation of not only the quadratic terms in the potential energy surface but also cubic and quartic terms. These are especially efficient using Density Functional Theory (DFT) methods such as B3LYP and allow use of much larger basis sets than in the past. Accordingly we have applied these modern tools to a reexamination of the structure and physical properties of $Be(BH_4)_2$ with the following objectives:

1. Determination of the most stable form of $Be(BH_4)_2$ and the existence and energies of any other bound forms.

2. Computation of the vibration-rotation parameters and vibrational infrared intensities at both harmonic and anharmonic levels.

3. Simulation of the observed room temperature and cooled jet spectra using the theoretical results obtained in 1 and 2.

The results of this thesis research are presented in the following chapters.

Chapter II : Potential Energy Surface of $Be(BH_4)_2$

Introduction

This thesis work has made extensive use of the Gaussian 09 program in an effort to understand the structure and properties of $Be(BH_4)_2$. Presented in this section is a brief summary of some of the important theoretical aspects of these quantum mechanical electronic structure calculations. Both pure *ab initio* and density functional methods have been employed, with the emphasis on the latter because experience has shown that these yield closer agreement between experimental and theoretical results for comparable or lower computing times. More extensive discussion of the theoretical basis for these calculations can be found in many texts. [27] [28] [29]

Ab initio Method

The fundamental equation for all electronic structure calculations is the Schrödinger Equation, which takes the (non-relativistic) form

$$H\Psi = \left(-\sum_{A} \frac{\nabla_A^2}{2M_A} - \sum_{i} \frac{\nabla_i^2}{2} + \sum_{A<B} \frac{Z_A Z_B}{R_{AB}} - \sum_{Ai} \frac{Z_A}{R_{Ai}} + \sum_{i<j} \frac{1}{r_{ij}} \right) \Psi = E\Psi \qquad (1)$$

where H is the exact Hamiltonian composed of the various terms in the parentheses. This equation is written in atomic units, with R or r representing the distance between any two particles, m_i the electron mass, and M_A and Z_A the mass and atomic number of the nuclei, respectively. The first sum in the parentheses is the kinetic energy of the nuclei and the second that of the electrons. The remaining terms are Columbic interactions that determine the potential energy of the charged particles in a molecule. The third and fifth sums are positive contributions to the energy from nuclear-nuclear and electron-electron repulsions, respectively. The fourth sum corresponds to the attraction between the nuclei and the electrons. This

negative term, along with the other positive terms, is responsible for the existence of a stable arrangement of these particles.

The *ab initio* methods make use of this exact Hamiltonian, with no adjustable parameters. For many-body systems, approximations are necessary to solve Schrodinger equation. One key approximation is the Born-Oppenheimer approximation, which simplifies the Hamiltonian by neglecting the kinetic energy of the nuclei and assuming that Ψ is a function of electron coordinates only. A second important approximation, the Hartree Fock (HF) approximation, assumes that the wavefunction can be written as a linear combination of spin orbitals of the form

$$\Psi(x_1, x_2) = {}^{1}/_{\sqrt{2}}\{\chi_1(x_1)\chi_2(x_2) - \chi_1(x_2)\chi_2(x_1)\}$$

where χ is a combined spatial and spin orbital and x expresses the position of the electron. Ψ can be written as a determinant, an advantage since the matrix form will preserve the antisymmetric nature of the wavefunction. This antisymmetric character for exchange of any two electrons (fermions) reflects Pauli Exclusion Principle. The representation of wavefunctions as determinants was first proposed by John Slater and hence this form of Ψ is called a Slater determinant.

In HF methods, the Hamiltonian can be taken to be exact. However, the wavefunction approximation results in significant errors because the determinantal form for Ψ neglects the correlation between electrons.[29] The correlation between electrons is such that the electrons tend to have low probability of being close together, with the consequence that the repulsive energy is less and the net energy is lower. A number of methods have been employed to account for electron correlation in *ab initio* calculations. One of the key methods to solve the correlation problem is configuration interaction, CI. The configuration interaction method endeavors to solve the nonrelativistic Schrödinger equation by using a linear combination of

symmetry adapted Slater determinants. All the determinants stemming from the same configuration have the same total quantum numbers but differ in their intermediate coupling.

$$|\psi\rangle = c_0|\Phi_0\rangle + \sum_{ra} c_a^r|\Phi_a^r\rangle + \sum_{a<b,r<s} c_{ab}^{rs}|\Phi_{ab}^{rs}\rangle + \sum_{r<s<t,a<b<c} c_{abc}^{rst}|\Phi_{abc}^{rst}\rangle + \cdots$$

where Φ_0 is a reference wavefunction, the *c*'s are coefficients, and Φ_a^r is the wave function resulting from replacing a spin orbital a of Φ_0 with a spin orbital r, etc. If this variational wavefunction includes all the possible spin orbitals, then a full configuration interaction is done. If it is chosen to change only one spin orbital, this is called single excitation configuration interaction (CI) or CIS. If two spin orbitals differ, it is a double excitation CI, denoted CID. Increasing the number of excitation has the disadvantage that it increases significantly the computing time. However, truncating the size of CI makes it size-inconsistent.[30] To solve the problem of size-inconsistency, many approaches were proposed. One of the most accurate solutions especially for medium size molecules is the coupled cluster (CC) method.

Coupled Cluster Method

Coupled cluster methods use an exponential ansatz to account for all the excitations determinant from the reference function.[31]

$$|\Psi\rangle = e^S|\Phi_0\rangle$$

$$S = \sum_{n=1}^{\infty} S_n$$

where S_n is the nth term exponential operator. As for CI methods, CC methods can be limited to be single excitations (CCS), double excitations (CCD) or both (CCSD). However, the nature of the exponential anstaz achieves the size-consistency. For example, CCD will take the form

$$|\Psi_{CCD}\rangle = exp(\hat{S}_2)|\Phi_0\rangle = \left(1 + \hat{S}_2 + \frac{1}{2}\hat{S}_2{}^2 + \frac{1}{3!}\hat{S}_2{}^3 + \cdots + |\Phi_0\rangle\right)$$

where $|\Phi_0\rangle$ is one of the standard basis sets in Gaussian. The expansion of the exponential to all of these terms would lead to accounting for all the possible interactions, e.g. $\hat{S}_2{}^2$ describes

pair-pair correlation and $\hat{S}_2^{\,3}$ correlates pair-pair-pair interactions.[32] Inclusion of these higher terms in the S expansion improves the property of size-consistency and makes the CC method more accurate than CI calculations. The CCSD(T) method, where the T implies a partial use of triple excitations, extrapolated to the complete basis set limit is sometimes called the "gold standard" of quantum calculations.[33] For this reason, and despite its time-intensive nature, a number of CCSD(T) calculations were done in this study, with the objective of determining the most reliable prediction of the lowest energy structure.

Density Functional Method

"It is an understatement to say that the Density Functional Theory has strongly influenced the evolution of quantum chemistry during the past 15 years; the term "revolutionalized" is perhaps more appropriate"[34].

Because of its accuracy and computational efficiency, Density Functional Theory (DFT) has proven an extremely useful tool in quantum calculations. This method depends on two principal theorems published by Hohenberg and Kohn in two seminal papers in 1964[35] and 1965[36]. DFT depends on the functional of charge density, $\rho(r)$ which uniquely defines the probability distribution of all the electrons. The first Hohenberg-Kohn (HK) theorem states that the density functional determines all the electronic properties of the ground state and its integral over all three spatial coordinates is equal to the total number of electrons, N.

$$\int \rho(r)dr = N$$

The second HK theorem applies the variational method to the density function $\rho = \psi^2$ to yield the lowest energy configuration. The details of the calculation are somewhat involved but are given in a number of references. [27] [28] [29] [37]

It should be noted that because the DFT method expresses the potential energy in terms of $\rho(r)$, the Hamiltonian is not exact and the variational results cannot be directly compared with those from true ab initio methods such as the Hartree Fock and Coupled Cluster methods. None the less, many studies have shown that DFT is capable of producing results in very good agreement with experiment at much less cost in computer time. Because of this efficiency, the method permits the computation of cubic and quartic anharmonic terms in the potential energy function, a capability not available at the time of William's calculations in 1996 but that has been utilized in the present work. This permitted computation of zero point energies, anharmonic vibrational frequencies and intensities, as well as a number of other vibration-rotation parameters that proved useful in the calculations of infrared spectra.

Calculations

The majority of the calculations that were done in this job utilized the Gaussian 09 B3LYP method. Multiple basis sets (cc-PVDZ, cc-PVTZ, cc-PVQZ, cc-PV5Z, aug-cc-PVTZ, N07d and N07T) were explored and the energy difference between the most stable forms were later extrapolated to the complete basis set (CBS) limit. After examining the results, it was found that the cc-PVTZ (polarized valence triple zeta) basis set, consisting of 294 primitive Gaussians, had both good accuracy and reasonable computing times. Therefore, along with the energies, the potential energy surface and the anharmonic frequency calculations were computed using this basis set.[38] However, to obtain the best prediction of the equilibrium structure, some additional calculations were done with the CCSD(T) method using the large cc-PVnZ basis sets, where n = D, T and Q indicates the use of double, triple or quadruple excitations. These calculations were done for both D_{2d} and D_{3d} structures and the energy difference was extrapolated to the complete basis set limit, as was done for the DFT calculations.

Results and Discussion

Equilibrium Energies (B3LYP/cc-PVTZ)

The energies of the various proposed structures shown in fig. 1.1 were examined with results generally consistent with earlier published work. Table 2.1 shows the results obtained using the DFT B3LYP method with a cc-PVTZ basis set. Three local minima were found on the potential energy surface of $Be(BH_4)_2$, corresponding to the "linear" D_{2d} and D_{3d} structures, along with a C_s triangular form (fig. 1.1 I, II and VI, respectively). The D_{2d} structure had lowest energy with the D_{3d} form 385 cm^{-1} higher. The stable triangular structure (VI) was 7936 cm^{-1} higher than the D_{2d} structure and accordingly would have very low concentration in an equilibrium mixture at room temperature.

The other structures did not turn out to be stationary points. The C_{3v} structure (Fig. 1.1 III) reverted during optimization to the D_{3d} structure. The other forms were found to correspond to maxima on the potential energy surface, with one or more negative vibrational frequencies. The lowest energy form of these, at 660 cm^{-1}, was the "linear" C_s structure IV which corresponds to a transition maximum with both a double and a triple hydrogen bridge around the beryllium center. Interestingly, at this maximum, the dipole moment along the symmetry axis was calculated to be 1.1 Debye, indicating appreciable charge rearrangement as the molecule converts from one nonpolar form to the other.

Table 2.1. B3LYP/cc-PVTZ energies of several proposed forms of $Be(BH_4)_2$

Structure	Energies (H)	ΔE^a (cm^{-1})	Place on PES

I	-69.313213	0	minimum
II	-69.311459	385	minimum
IV	-69.310204	660	transition state (1)[b]
V	-69.256877	12364	saddle point (3) [b]
VI	-69.277055	7936	minimum
VII	-69.083061	50512	saddle point (4) [b]

[a] ΔE is the energy of a given structure relative to the D_{2d} structure.
[b] Energy maxima with the number of negative vibrational frequencies indicated in parentheses.

Potential energy surface (B3LYP/cc-PVTZ)

Two B3LYP/cc-PVTZ potential energy surfaces were calculated using the BH_4 twisting and tumbling coordinates shown in Figure 2.1. Only the D_{2d} and D_{3d} local minima for a "linear" structure are shown in the surfaces; the minimum for the triangular structure (Fig. 1.1 VII) was much higher in energy. The three "linear" structures (Fig. 1.1 I, II and IV) differ from each other in the orthogonal tumbling angles Θ_1 and Θ_2 (Fig. 2.1 a). The PES was generated by independently scanning each of these angles, with optimization of all other structural parameters at each grid point. The result is shown in Figure 2.2. The D_{2d} minimum occurs at $\Theta_1 = \Theta_2 = 120.0^\circ$ while for the D_{3d} minimum, $\Theta_1 = \Theta_2 = 65.0^\circ$. The highest point on this surface, which is a saddle point of order two, is 773 cm^{-1} higher than the D_{2d} structure. Interestingly, the lowest energy path between these two structures occurs at 553 cm^{-1}, near the transition structure IV, with $\Theta_1 = 120.0^\circ$, $\Theta_2 = 77.0^\circ$. This indicates that independent or synchronous rotation of the tumbling angles involves comparable energies, suggesting that there is little coupling between the BH_4 units.

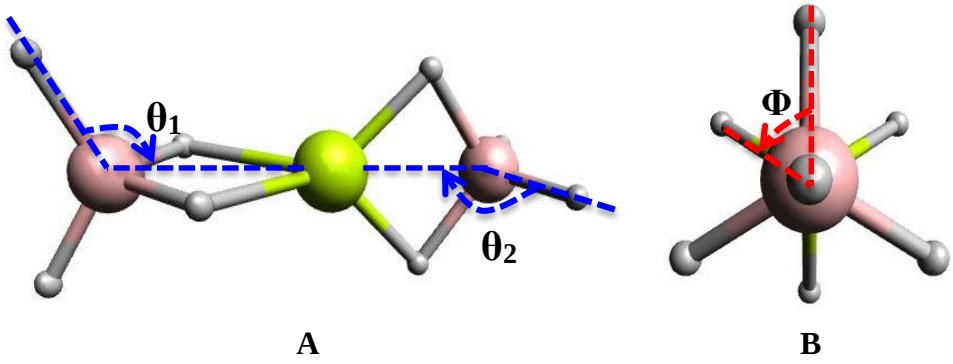

Figure 2.1: A. Orthogonal BH_4 tumbling angles. B. Torsion angle between triple (or double) bridge units.

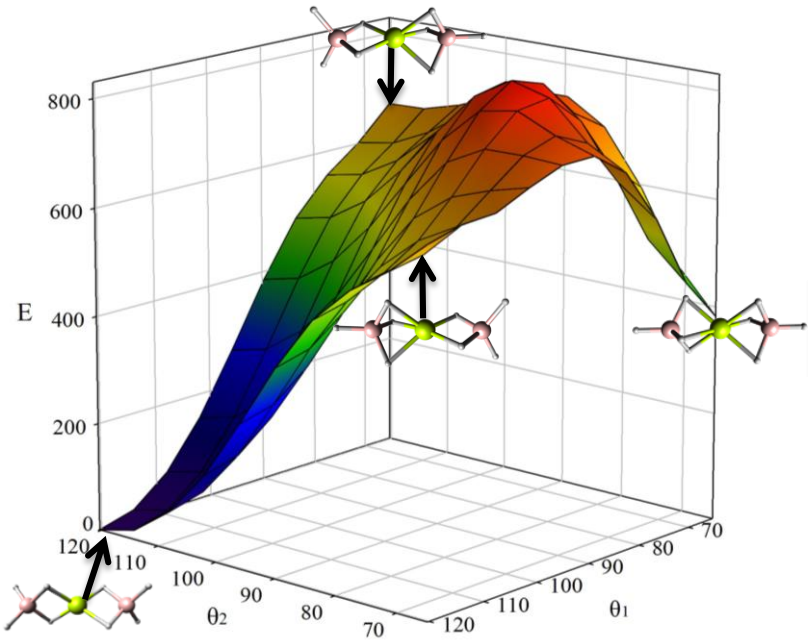

Figure 2.2: Potential energy surface for two tumbling angles changing independently.

The second PES exploration (Fig. 2.3a, b) performed in this work was to investigate the energy variation as both the tumbling and torsional angles were changed. This surface was generated by optimizing each structure at a specific value of the tumbling angles $\Theta = \Theta_1 = \Theta_2$ (synchronous tumbling). Later, each optimized structure was held rigid as the torsional angle ϕ was scanned from 0-360°. ϕ (Fig. 2.2 b) represents the torsion angle of the two BH_4 groups, with $\phi = 0$ corresponding to eclipsed forms of the BH_4 units in either the D_{3d} or D_{2d} structures.

The high torsional energy barrier (3323 cm^{-1}) for the D_{2d} form is because all hydrogen bridge bonds in the two units are in the same plane. This barrier is much less in the D_{3d} case (480 cm^{-1}). The dotted line in Fig. 2.3a shows the low energy tumbling, torsional path between the D_{3d} and D_{2d} structures and a side view of this surface is shown in Fig. 2.3. When the torsional angle was varied, the barrier maximum is 1176 cm^{-1}, corresponding to a synchronous change of the tumbling angles to 87˚. However, this barrier will decrease if all coordinates are allowed to relax; for example in fig 2.2 the relaxed energy is about 420 cm^{-1}. Regardless, it seems clear from these surfaces that the low energies of the transition paths are consistent with a highly fluxional nature for $Be(BH_4)_2$.

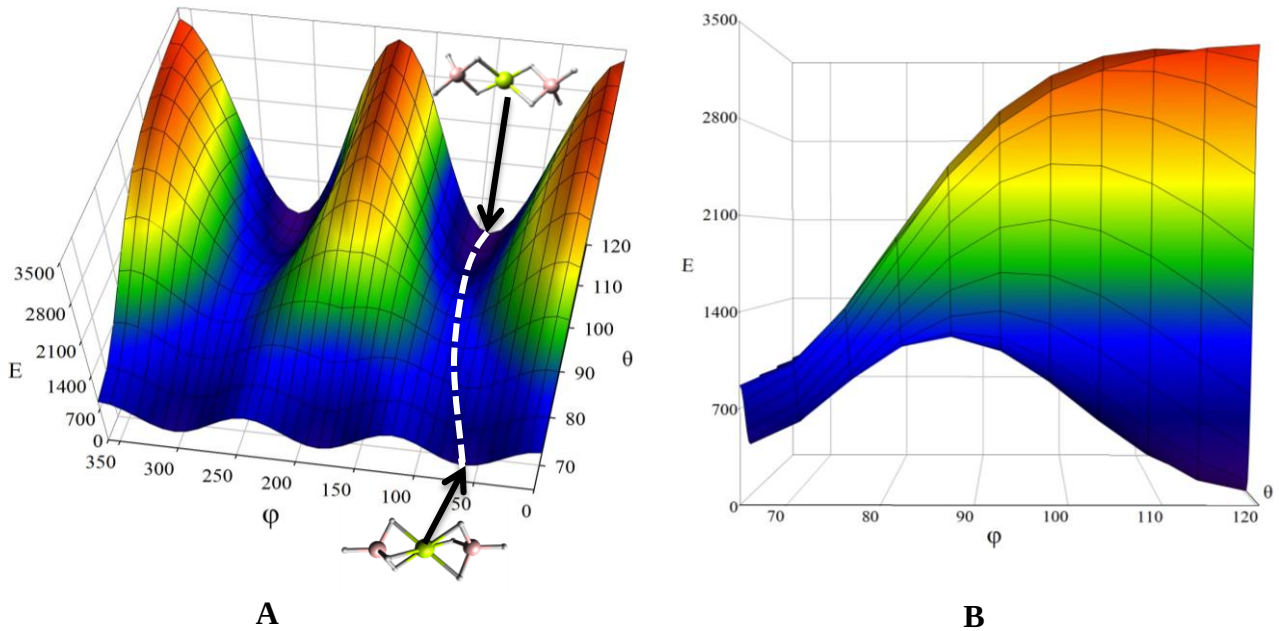

Figure 2.3. A. Potential energy surface of the torsional and tumbling angle, where θ is the synchronous change of the angles θ_1 and θ_2. B. Side view of the path between D_{3d} and D_{2d} structures (The minimum energy path corresponds to the dashed line in A).

Effect of Basis Size and Zero Point Energy (ZPE)

The effect of basis set size was then explored using the B3LYP method, yielding the results shown in Table 2.2. In all cases, minima were found for both D_{2d} and D_{3d} forms and, except for the cc-PVDZ basis set, the D_{2d} structure was lowest in energy. Figure (2.4 A) displays the energy of the D_{2d} and the D_{3d} forms as a function of the number of primitive Gaussians for the cc-PVnZ basis sets with n = 2 (D), 3(T), 4(Q), 5. In all cases the energy appears to be converging and, on extrapolation to the basis set limit[38], the D_{3d} - D_{2d} equilibrium energy difference is 353 cm^{-1}.

Table 2.2. B3LYP energies of the D_{3d} and D_{2d} forms of $Be(BH_4)_2$ using different basis sets

Basis sets	Primitive gaussians	D_{2d}		D_{3d}		D_{3d}-D_{2d} (cm^{-1})	
		E_{elec} (H)	[a]ZPE (cm^{-1})	E_{elec} (H)	ZPE (cm^{-1})	E_{elec}	ZPE
N07D	150	-69.289226	18101	-69.288277	17895	208	-206
cc-PVDZ	155	-69.274165	17924	-69.274266	17775	-22	-149
N07D diff	158	-69.289784	18111	-69.288828	17903	210	-207
N07T	237	-69.314948	18157	-69.312702	17878	493	-279
cc-PVTZ	294	-69.313213	18160	-69.311459	17891	373	-258
spaug-cc-PVTZ	338	-69.313441	18154	-69.311695	17891	383	-262
cc-PVQZ	560	-69.319664	18165	-69.317949	17906	376	-259
cc-PV5Z	1031	-69.321767	18167	-69.320086	17907	369	-260
CBS [b]	∞					353	-255

[a] ZPE is the zero point energy obtained using calculated harmonic frequencies.

[b] Obtained by extrapolation of the cc-PVnZ basis sets to the complete basis set limit.

Although the DFT calculations thus indicate that the most stable equilibrium structure is the D_{2d} form, the molecules must reside in the ground state level at 0 K and it is conceivable that this level could be lower for the D_{3d} form compared to that for the D_{2d} structure. The position of the ground state levels is determined by the zero point energy (ZPE), which is

simply half the sum of the vibrational frequencies of the 27 normal modes. Using harmonic vibrational frequencies, this ZPE sum is shown in Table 2.2 and the effect of adding it to the equilibrium energies is displayed in Fig. 2.4 B. It is seen that D_{3d} - D_{2d} energy difference narrows considerably and, at the complete basis set limit, the difference is only 97 cm^{-1}. Ideally, anharmonic frequencies should be used in calculating the ZPE sums but these were not available for the larger basis sets; in the cases where they were calculated, comparable narrowing of the D_{3d} - D_{2d} energy difference was observed.

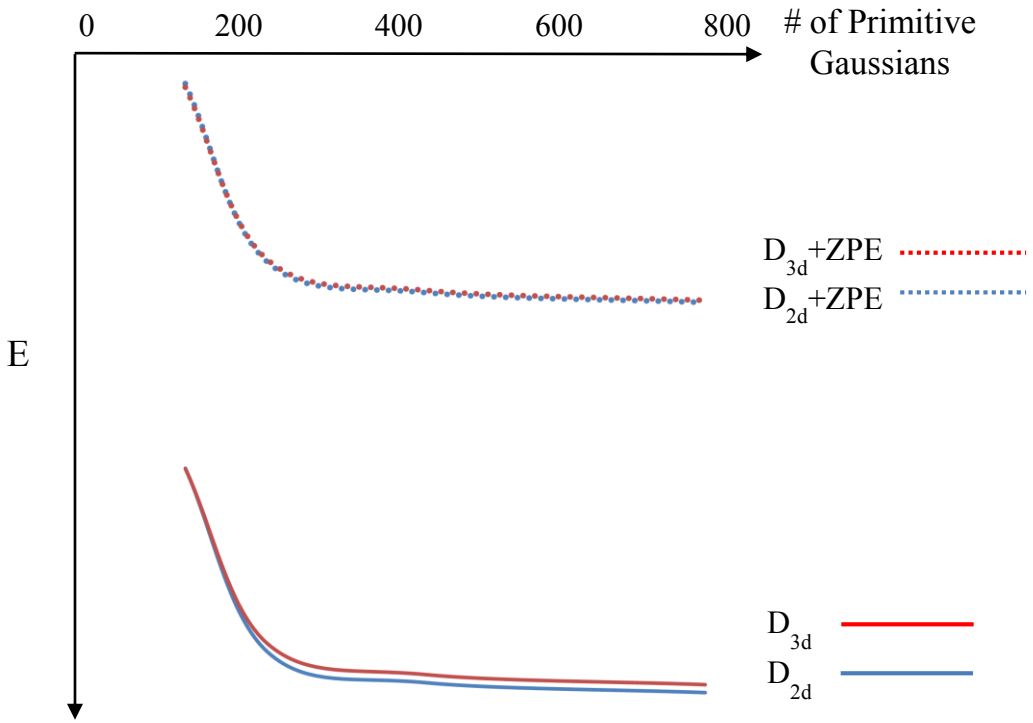

Figure 2.4: Results from B3LYP/cc-PVnZ calculations of E_{elec} and E_{elec}+ZPE

CCSD(T) Calculations

Although the B3LYP (DFT) calculations consistently predict the D_{2d} form of $Be(BH_4)_2$ to be the lowest energy structure, they also show that the D_{3d} form corresponds to a local minimum of only slightly higher energy. This slight difference, judged to be comparable to the accuracy of the DFT method, led us to examine the predictions of the Coupled Cluster

method. In particular, the CCSD(T) method, unlike the DFT method, utilizes the true Hamiltonian and the results from CCSD(T) calculations are generally believed to more accurately account for electron correlation effects. They are, however, much more demanding of computer time since they include the effect of single, double and some triple excitations. The result is that it is impractical to compute anharmonic contributions to the potential energy and even harmonic vibrational frequencies are only feasible for small basis set sizes. Accordingly the focus was on obtaining the equilibrium energies of both D_{2d} and D_{3d} forms for the basis set series cc-PVDZ, cc-PVTZ and cc-PVQZ.

The results of these CCSD(T) calculations, shown in Table 2.3, show a reversal of the D_{2d} and D_{3d} energy ordering, with the D_{3d} form favored for the larger basis sets. In the CBS limit, the difference is 90 cm^{-1}. The effect of the harmonic ZPE in determining the relative positions of the ground state levels for both forms could only be calculated for the smallest cc-PVDZ basis set but, as for the DFT results, it results in a favoring of the D_{3d} form by 206 cm^{-1}. A comparable favoring would be expected in the CBS limit.

Table 2.3: Calculated energies of $Be(BH_4)_2$ using CCSD(T) method

Basis sets	D_{2d}	D_{3d}	Difference cm^{-1}	Time (hours)
cc-PVDZ	-68.990633	-68.988848	392	3
cc-PVTZ	-69.070508	-69.070200	68	54
cc-PVQZ	-69.090966	-69.091125	-35	157
CBS			-90	

Table 2.4: The optimized parameters of the two minima on PES, D_{2d} and D_{3d}

Parameters[a]	D_{2d}				D_{3d}			
	B3LYP		CCSD(T)		B3LYP		CCSD(T)	
	cc-PVTZ	cc-PVQZ	cc-PVTZ	cc-PVQZ	cc-PVTZ	cc-PVQZ	cc-PVTZ	cc-PVQZ
Be-B	1.839	1.837	1.847	1.842	1.719	1.717	1.725	1.721
Be-H_b	1.464	1.462	1.470	1.467	1.641	1.639	1.640	1.636
B-H_t	1.189	1.189	1.193	1.192	1.177	1.177	1.180	1.179
B-H_b	1.280	1.279	1.285	1.283	1.241	1.241	1.247	1.245
H_t' B H_t[b]	119.4	119.4	120.1	120.1				
H_t' B H_b'	108.0	108.0	107.8	107.8	115.0	115.0	115.3	115.4
Be B H_t	120.3	120.3	120.0	120.0	*180*[c]	*180*	*180*	*180*
H_b Be B H_t[b]	*180*	*180*	*180*	*180*				
H_t' B B H_t'	*90*	*90*	*90*	*90*				
H_t' B B H_t"	*-90*	*-90*	*-90*	*-90*				

[a] Distances are measured in Å.

[b] t stands for terminal, b for bridging, H' and H" are on different BH_4^- units.

[c] Italicized angles are fixed by symmetry.

Conclusion

The calculations presented here employed higher level methods and larger basis sets than the previous theoretical studies of $Be(BH_4)_2$. Only three of the proposed structures were found to be minima on the potential energy surface of the compound, the D_{2d}, D_{3d} and C_s forms (fig. 1.1 I, II and VI), with the latter much higher in energy. In the complete basis set limit, the DFT method indicates that the D_{2d} is 353 cm^{-1} lower than the D_{3d} form. The reverse ordering is found from the Coupled Custer calculation, but with a difference in energy of only 90 cm^{-1}. In all cases, inclusion of the zero point energy tends to lower the ground state energy of the D_{3d} form relative to that of the D_{2d} form. Although the energy differences are small, the CCSD(T) results are believed to be the most reliable, indicating that the lowest energy form of $Be(BH_4)_2$ is the triply bridged D_{3d} arrangement.

The predicted bond lengths and angles of both D_{2d} and D_{3d} forms are listed in Table 2.4 for both B3LYP and CCSD(T) methods using both cc-PVTZ and cc-PVQZ basis sets. As can be seen, the structural results do not differ appreciably for the different methods or choice of basis set. However, on going from D_{2d} to D_{3d} geometries, significant structural changes occur for the BBe and BeH_b separations; the former drops by about 0.12 Å while the latter increases by about 0.17 Å. Concurrently, the difference between the bridge and terminal BH bond lengths decreases slightly, in the direction expected for a more ionic BH_4^- anion. This result, plus the low barriers for interconversion of the D_{2d} and D_{3d} forms, suggests that, even in the vapor phase $Be(BH_4)_2$ might be viewed as a Be^{2+} cation with two BH_4^- anions nearly freely rotating on opposite sides. Alternatively, a more likely intermediate description would correspond to a BH_4^- anion bound to a $BeH_2BH_2^+$ cation, as implied by structure IV. This structure was found to be a low energy transition state in the DFT calculation but was not a stationary state. In future work, it would be interesting to see if such a form is bound in the

more lengthy CCSD(T) calculations. If there is an appreciable amount of this polar form in the vapor, this could account for the electric deflection results. It also could be that, given the fluxional nature of $Be(BH_4)_2$ a significant dipole could be induced by the electric field in the deflection experiment.

Finally, it is interesting to note that the choice of basis set or quantum method has relatively little effect on the predicted structural parameters or the zero point energies of $Be(BH_4)_2$. This offers hope that the quantum calculations can give reasonable values for the potential constants, particularly for the modes that do not directly involve the torsional modes. This aspect is explored further in the next chapter where an effort is made to relate the theoretical results to experiment.

Chapter III: Spectrum Simulation

Introduction

In this chapter, results are given from B3LYP/cc-PVTZ electronic structure calculations at the anharmonic level using the AnHarm/VibRot options of Gaussian 09. These consist of the following vibration-rotation parameters for both D_{3d} and D_{2d} structures of $Be(BH_4)_2$:

a. Vibrational frequencies. These include the 27 fundamental values as well as values of selected binary combinations, both at the harmonic and anharmonic level.

b. Harmonic and anharmonic infrared intensities of all transitions from the ground state to the fundamental and overtone/combination levels obtained in a.

c. *A*, *B*, and *C* rotational constants for the equilibrium structure and for the ground state as well as the changes in these for all of the levels obtained in a.

d. D_J, D_{JK} and D_K centrifugal distortion constants for the equilibrium structure.

e. ζ Coriolis constants for the vibration-rotation interaction of all fundamentals.

These constants represent new or improved estimates compared to those available in previous attempts to understand the vibrational and vibration-rotation spectra of $Be(BH_4)_2$ in the vapor phase at room temperature and in argon matrices at 20 K. Efforts are also made to simulate resolved infrared vibration-rotation features seen in diode laser scans of a narrow region of the bridge bond stretching region for $Be(BH_4)_2$ cooled to 10-20 K in an argon jet.

Vibrational Model

The basic elements of vibration-rotation theory are well understood and can be found in many texts. [39] [40] We give here only a brief discussion of some of the principles and equations relevant to this work. For $Be(BH_4)_2$ with N=11 atoms, one expects 3N-6 = 27 vibrational normal modes. From group theory, each of these must correspond to one of the symmetry species of the point group for the molecule, which is D_{3d} or D_{2d}. The harmonic frequencies of

these modes are calculated using the quadratic terms in the vibrational potential function, yielding in the case of a diatomic molecule the simple energy expression,

$$E(\mathrm{v}) = (\mathrm{v}+ ½)\hbar\omega = (\mathrm{v}+ ½)\hbar(k/\mu)^{½}$$

where v is the vibrational quantum number and ω is the harmonic vibrational frequency, k is the quadratic force constant and μ is the reduced mass. This result predicts a simple set of energy levels spaced evenly by $\hbar\omega$, with the fundamental transition corresponding to the transition from the ground state (v=0) to the first level (v=1). In actual molecules, small anharmonic terms in the potential cause the level spacings to decrease as v increases. To account for this, small higher power terms such as $-(\mathrm{v}+ ½)^2\hbar\omega x_e$ are added to the energy expression. The anharmonic value ν for the fundamental transition is thus lowered, typically by a few percent, to $\nu = \omega - 2\omega x_e$.

For nonlinear polyatomic molecules, there will be 3N-6 normal modes and each will have a level pattern similar to that of a diatomic molecule, but with a more complex form for the reduced mass. With the "Freq" option of the Gaussian program, appropriate mass terms are computed, along with the quadratic potential energy values. These yield a prediction of the harmonic frequencies and of the infrared and Raman intensities of the fundamental transitions. Including the recent "AnHarm" option in Gaussian requires considerably more computation time but yields values of the cubic and quadratic potential constants, which then allow prediction of the anharmonic frequencies and intensities.

Not all of the fundamental modes are observed in the infrared spectrum because not all of them fulfill the requirement for an infrared transition, which is that the mode must involve an oscillating dipole moment for interaction with oscillating electromagnetic field of the infrared wave. For a given allowed fundamental mode, the transition occurs from the ground vibrational level (v=0) to a state in which the same vibrational quantum number increases by

1. For an overtone transition this change is 2. The intensity that is zero in the harmonic approximation can be nonzero when one takes into account anharmonic effects on both the normal mode and on the dipole moment function. Similarly, transition to combination states can have nonzero intensity in the anharmonic case. The predicted transitions and intensities are of considerable aid in interpreting the observed vibrational spectra for a molecule and are so employed here for $Be(BH_4)_2$.

Rotational Model

In the gas phase, all molecules rotate and the model used to describe the rotational energies is the rigid rotor model, in which the molecular configuration is fixed, yielding *A, B, C* rotational constants determined by the moments of inertia $I_a < I_b < I_c$

$$A = \frac{h}{8I_a\pi^2c} \quad > \quad B = \frac{h}{8I_b\pi^2c} \quad > \quad C = \frac{h}{8I_c\pi^2c}$$

For a prolate symmetric top such as $Be(BH_4)_2$, $B = C$ and the energy levels are given by the expression[41]

$$F(J,K) = BJ(J+1) - (A-B)K^2$$

where the rotational quantum number $J = 0, 1, 2$ .. characterizes the total angular momentum vector and $K = 0, \pm1, \ldots \pm J$ gives the possible projections of vector J on the molecule fixed symmetry axis.

Although this rigid rotor model is quite good, corrections are needed to properly account for high resolution spectra. Two such corrections are due to vibration rotation coupling and centrifugal distortion. The former causes small changes in the rotational constants for different vibrational levels and are characterized by the vibration-rotation coupling constants, $\alpha_A = A''-A'$, $\alpha_B = B''-B'$ where the " symbol denotes the lower state. Even in a given vibrational

state, rotation of a molecule will extend the "rigid" bonds slightly and this is accounted for by including D_J, D_{JK} and D_K centrifugal distortion constants. This yields the energy relation:

$$F(J,K) = BJ(J+1) + (A-B)K^2 - D_J J^2(J+1)^2 - D_{JK}J(J+1)K^2 - D_K K^4$$

where A and B include the α corrections. This expression adequately describes the ground vibrational state and all states that do not involve excitation of degenerate vibrations (the latter are states of symmetry E). For the E states, coupling between the x and y components of the vibration produce a rotary-type motion that gives a vibrational angular momentum characterized by the quantum number $l = \pm 1$. This requires an added term $-2\zeta AKl$ in the $F(J,K)$ expression for all degenerate vibrational levels.[42] Values for all of these parameters can be obtained from the Gaussian program using the Freq = AnHarm, VibRot options.

Theory predicts that two types of vibration-rotation transitions can occur in prolate top molecules. The first involves an oscillating dipole along the A symmetry axis and is termed a parallel band with selection rules $\Delta K = 0$, $\Delta J = -1, 0, +1$, with the latter termed P, Q, R transitions, respectively. In the case of a transition from the ground state to a vibrational level of symmetry E, the oscillating dipole is perpendicular to the symmetry axis, giving rise to a perpendicular band in which the selection rules are $\Delta K = \pm 1$, $\Delta J = -1, 0, +1$. As will be seen in simulations below, the two types of bands have quite different structures.

The Gaussian calculations give quite good estimates of all of the parameters described above. They also treat one other common perturbation to the vibrational levels, i.e. Fermi Resonance. This occurs whenever a fundamental level has the same symmetry as that of a nearby overtone or combination state. Cubic potential terms cause a mixing of these states, resulting in two effects. First, the energy levels repel, the higher level gets higher and the lower level gets lower. Second, due to the mixing of the states, the intensities change, with the fundamental getting weaker and the overtone or combination transition getting more intense.

If appreciable, Fermi resonance can produce two medium intensity, nearby, features rather than one weak and one strong band, making the interpretation of the spectrum more difficult.

Theoretical Results

All calculations of the vibration-rotation parameters were performed with Gaussian 09 and the DFT B3LYP method using the cc-PVTZ basis set. Ideally, the coupled cluster method would have been preferred but the AnHarm and VibRot options are not available for this method and even calculation of harmonic vibrational frequencies are very time consuming. For example, such a calculation for the D_{3d} structure took over 13 days using a fast PC with four coprocessors. A similar calculation using the B3LYP method took only 5 minutes and gave quite similar values for most of the vibrational modes. Similar agreement was seen in comparisons for the D_{2d} frequencies calculated for the cc-PVDZ basis set so it is believed that the DFT results give a reasonable representation of the harmonic potential around the D_{3d} and D_{2d} minima. The B3LYP/cc-PVTZ anharmonic calculations took much longer than the harmonic ones, typically 1 days versus 5 minutes. These B3LYP/cc-PVTZ results are shown in Tables 3-1 to 3-5 and these parameters were used in the spectral simulations described below. For the latter, the theoretical results were used as input parameters to the Art Maki program SYMROT, which was modified to provide transition intensities. Generation of a spectrum and comparison with experiment was done using the software program IGOR.

Table 3.1: Theoretical rotational and centrifugal distortion constants[a] of $Be(BH_4)_2$

	D_{2d}	D_{3d}
A_e	2.009641	2.200897
B_e	0.157335	0.178527
A_{00}	1.977678	2.140540
B_{00}	0.155012	0.173488
D_J	5.807390E-08	6.015838E-08
D_{JK}	3.473233E-06	1.061199E-06
D_K	5.275912E-06	8.662975E-06

[a] The values are from B3LYP/cc-PVTZ calculations using Gaussian 09 b.1 and d.1 with Anharm/Vibrot options

Table 3.2: Theoretical rovibrational parameters[a] (cm^{-1}) of the fundamental levels of D_{2d} form of $Be(BH_4)_2$

			Frequency(cm^{-1})			Intensities(Km/mol)		ΔA = A' - A" ($\times10^{-3}$)	ΔB = B' - B" ($\times10^{-3}$)	
Mode	Sym	Activity	harm	anharm		I(harm)	I(anharm)			$A'\zeta$
ν_1	a_1	R	2586.7	2486.3		0	0	-7.433	-0.081	
ν_2	a_1	R	2111.1	2008.2	***2032.8***	0	0	-1.083	-0.329	
ν_3	a_1	R	1616.3	1493.8		0	0	-4.966	-0.596	
ν_4	a_1	R	1157.5	1135.4		0	0	114.467[b]	0.042	
ν_5	a_1	R	503.2	493.9		0	0	0.051	-0.291	
ν_6	a_2		1131.0	1105.3		0	0	-120.164[b]	-0.052	
ν_7	b_1	R	1136.4	1109.7	***1110.0***	0	0	-175.688[c]	-0.064	
ν_8	b_1	R	305.8	286.0		0	0	-4.396	-0.069	
ν_9	b_2	ir/R	2584.7	2484.5		84	68	-7.362	-0.080	
ν_{10}	b_2	ir/R	2088.9	2005.8	***2026.9***	268	159	-0.289	-0.318	
ν_{11}	b_2	ir/R	1675.6	1511.4	***1523.4***	937	814	-7.146	-0.756	
ν_{12}	b_2	ir/R	1153.3	1130.9		51	51	170.996[c]	0.030	
ν_{13}	b_2	ir/R	974.8	937.1		112	94	-0.106	-1.032	
ν_{14}	e	ir/R	2657.6	2536.9	***2532.8***	140	127	-5.176	-0.055	0
ν_{15}	e	ir/R	2044.4	1941.4	***1927.5***	181	98	-1.426	-0.622	-0.031797
ν_{16}	e	ir/R	1579.9	1486.9		10	4	1.201	-0.965	-0.114177
ν_{17}	e	ir/R	1026.6	1035.2		2	2	-6.807	-0.076	0
ν_{18}	e	ir/R	872.2	818.8		12	10	1.009	-0.442	-0.033755
ν_{19}	e	ir/R	353.7	335.9		26	28	10.253	0.526	-0.950177
ν_{20}	e	ir/R	112.6	121.2		29	24	-9.477	1.107	-0.769027

[a] The values are from B3LYP/cc-pVTZ calculations using Gaussian 09 b.1 and d.1 with Anharm/Vibrot options. Anharmonic frequencies in bold italics are from Gaussian and include shifts caused by Fermi resonance.

[b]Values too large due to a Coriolis resonance between ν_4 and ν_6. The sum $\Delta A_4 + \Delta A_6$ is -5.697 cm^{-1}

[c]Values too large due to a Coriolis resonance between ν_7 and ν_{12}. The sum $\Delta A_7 + \Delta A_{12}$ is -4.692 cm·

Table 3.3: Theoretical rovibrational parameters (cm^{-1}) of the overtones and combination bands of D_{2d} form of $Be(BH_4)_2$

			Frequency(cm^{-1})		Intensities(Km/mol)	ΔA = A' - A"	ΔB = B' - B"
Mode	Sym.	Activity	harmonic	anharmonic	I(anharm)	($\times10^{-3}$)	($\times10^{-3}$)
$2\nu_4$	a_1	R	2315.1	2265.9	0	228.933	0.084
$2\nu_{12}$	a_1	R	2306.6	2257.2	0	341.992	0.060
$2\nu_7$	a_1	R	2272.8	2219.6	0	-351.375	-0.129
$2\nu_6$	a_1	R	2262.1	2210.4	0	-240.328	-0.103
$\nu_8+\nu_2$	b_1	R	2416.8	2298.0	0	-5.479	-0.397
$\nu_{19}+\nu_{15}$	$a_1+a_2+b_1+b_2$		2398.1	2271.3	0	8.827	-0.095
$\nu_{19}+\nu_{15}$	$a_1+a_2+b_1+b_2$	ir	2398.1	2271.3	2	8.827	-0.095
$\nu_{19}+\nu_{15}$	$a_1+a_2+b_1+b_2$	ir	2398.1	2264.8	2	8.827	-0.095
$\nu_{19}+\nu_{15}$	$a_1+a_2+b_1+b_2$		2398.1	2264.8	0	8.827	-0.095
$\nu_{10}+\nu_8$	a_2		2394.6	2279.7	0	-4.685	-0.387
$\nu_{16}+\nu_8$	e	ir/R	2350.2	2220.2	1	-5.822	-0.690
$\nu_{17}+\nu_{12}$	b_2	ir	2310.8	2256.7	7	285.463	0.072
$\nu_7+\nu_4$	b_1	R	2293.9	2246.2	0	-61.221	-0.023
$\nu_{12}+\nu_7$	a_2		2289.7	2242.4	0	-4.691	-0.035
$\nu_6+\nu_4$	a_2		2288.6	2242.2	0	-5.697	-0.010
$\nu_6+\nu_{12}$	b_1	R	2284.4	2237.0	0	50.832	-0.022
$\nu_6+\nu_7$	b_2	ir	2267.5	2215.7	5	-295.852	-0.116
$\nu_{20}+\nu_2$	e	ir/R	2223.7	2131.7	11	-10.559	0.779
$\nu_{20}+\nu_{10}$	e	ir/R	2201.5	2114.6	1	-9.765	0.789
$\nu_{17}+\nu_4$	e	ir/R	2184.1	2139.2	1	107.660	-0.035
$\nu_{17}+\nu_{12}$	e	ir/R	2179.9	2135.2	0	164.190	-0.046
$\nu_{17}+\nu_7$	e	ir/R	2163.0	2118.5	0	-182.494	-0.141
$\nu_{17}+\nu_6$	e	ir/R	2157.6	2113.5	6	-126.970	-0.128

[a] The values are from B3LYP/cc-pVTZ calculations using Gaussian 09 b.1 and d.1 with Anharm/Vibrot options. Anharmonic frequencies in bold italics are from Gaussian and include shifts caused by Fermi resonance. Values of $\Delta A > 50\times10^{-3}$ indicate that corrections for Coriolis resonances are needed.

Table 3.4: Theoretical rovibrational parameters (cm^{-1}) of the fundamental levels of D_{3d} form of $Be(BH_4)_2$

			Frequency(cm^{-1})			intensities(Km/mol)		ΔA = A' - A" ($\times10^{-3}$)	ΔB = B' - B" ($\times10^{-3}$)	
Mode	Sym.	Activity	harm	anharm		I(harm)	I(anharm)			$A'\zeta$
ν_1	a_{1g}	R	2727.7	2625.9	***2623.6***	0.0	0.0	-1.152	-0.312	
ν_2	a_{1g}	R	2312.7	2152.5	***2190.2***	0.0	6.6	-7.492	-0.197	
ν_3	a_{1g}	R	1325.2	1253.4		0.0	0.0	-4.488	-2.356	
ν_4	a_{1g}	R	594.8	520.8	***543.4***	0.0	0.0	-0.620	-0.328	
ν_5	a_{1u}		195.5	162.8		0.0	0.0	-2.350	-0.350	
ν_6	a_{2u}	ir	2728.2	2626.2	***2624.0***	70	54	-1.096	-0.316	
ν_7	a_{2u}	ir	2298.7	2149.1	***2175.3***	209	177	-6.994	-0.194	
ν_8	a_{2u}	ir	1276.4	1211.6		53	61	-1.256	-1.338	
ν_9	a_{2u}	ir	1046.1	1089.3		747	270	-4.385	-1.315	
ν_{10}	e_g	R	2278.2	2135.8	***2138.7***	0	1	-0.174	-0.283	-0.11877
ν_{11}	e_g	R	1343.6	1266.0	***1285.4***	0	0	-6.597	0.696	0.29898
ν_{12}	e_g	R	1128.8	1108.3		0	0	-7.621	-0.300	-1.06426
ν_{13}	e_g	R	415.2	324.1		0	0	-6.779	-0.900	1.57293
ν_{14}	e_u	ir	2314.8	2174.7		262	219	-0.850	-0.286	0.12055
ν_{15}	e_u	ir	1317.6	1261.4	***1270.5***	13	12	-5.873	0.248	0.27276
ν_{16}	e_u	ir	1138.0	1122.3		35	33	-7.057	-0.279	-1.08654
ν_{17}	e_u	ir	413.8	318.7		12	7	-7.238	-0.926	-1.55122
ν_{18}	e_u	ir	288.1	275.4		50	56	-3.160	0.344	-2.02549

[a] The values are from B3LYP/cc-PVTZ calculations using Gaussian 09 b.1 and d.1 with Anharm/Vibrot options. Anharmonic frequencies in bold italics are from Gaussian and include shifts caused by Fermi resonance.

Table 3.5: Theoretical rojjjvibrational parameters (cm^{-1}) of the overtones and combination bands of D_{3d} form of $Be(BH_4)_2$

			Frequency(cm^{-1})			Intensity(Km/mol)	ΔA = A' - A" ($\times10^{-3}$)	ΔB = B' - B" ($\times10^{-3}$)
Mode	Sym.	Activity	harm	anharm		anharmonic		
$2\nu_{16}$	$a_{1g}+e_g$		2276.0	2239.5	***2240.4***	0	-14.115	-0.559
$2\nu_{12}$	$a_{1g}+e_g$		2257.5	2214.0	***2210.3***	0	-15.244	-0.600
$2\nu_9$	a_{1g}	R	2092.2	2172.3		0	-8.770	-2.629
$\nu_9+\nu_8$	a_{1g}	R	2322.5	2294.9		0	-5.641	-2.653
$\nu_{16}+\nu_{12}$	$a_{1u}+a_{2u}$	ir	2266.8	2246.8		5	-14.678	-0.580
$\nu_{16}+\nu_{12}$	$a_{1u}+a_{2u}$	ir	2266.8	2220.5	***2220.3***	5	-14.678	-0.580
$\nu_{16}+\nu_{12}$	e_u	ir	2266.8	2226.9		8	-14.678	-0.580
$\nu_{16}+\nu_9$	e_g	R	2184.1	2203.7		0	-11.442	-1.594
$\nu_{12}+\nu_9$	e_u	ir	2174.9	2187.8		0	-12.006	-1.614

[a] The values are from B3LYP/cc-PVTZ calculations using Gaussian 09 b.1 and d.1 with Anharm/Vibrot options. Anharmonic frequencies in bold italics are from Gaussian and include shifts caused by Fermi resonance.

Results and Discussion

Vibrational Spectra

It is of interest to compare the anharmonic vibrational frequencies and intensities given in Tables 3.2-3.5 with the experimental spectra observed for $Be(BH_4)_2$. Figure 3.1A offers such a comparison, with the top trace corresponding to an infrared spectrum of the vapor at room temperature recorded in 1972 by Nibler.[15] Displayed at the bottom are stick spectra based on the present anharmonic results for both D_{3d} and D_{2d} forms, information not available at the time of the experimental measurements. Although not a perfect match, it is seen that each strong absorption in the experimental spectrum corresponds to one of the intense vibrational bands predicted for the D_{3d} and/or the D_{2d} structures. For example, the most intense D_{2d} fundamental is predicted at 1511 cm^{-1}, very near the strong feature at 1550 cm^{-1}. Other strong D_{2d} bands are predicted at 2533, 2027 and 1928 cm^{-1}, also regions of strong infrared absorption in the experimental spectrum. None of these absorptions are predicted for the D_{3d} model; instead strong features are calculated to occur at 2624, 2175 and 1089 cm^{-1}. Features near these values are also seen in the infrared spectrum but are not expected from the D_{2d} calculations. Thus it seems quite clear that the spectrum at room temperature is a superposition of contributions from both D_{3d} and D_{2d} forms.

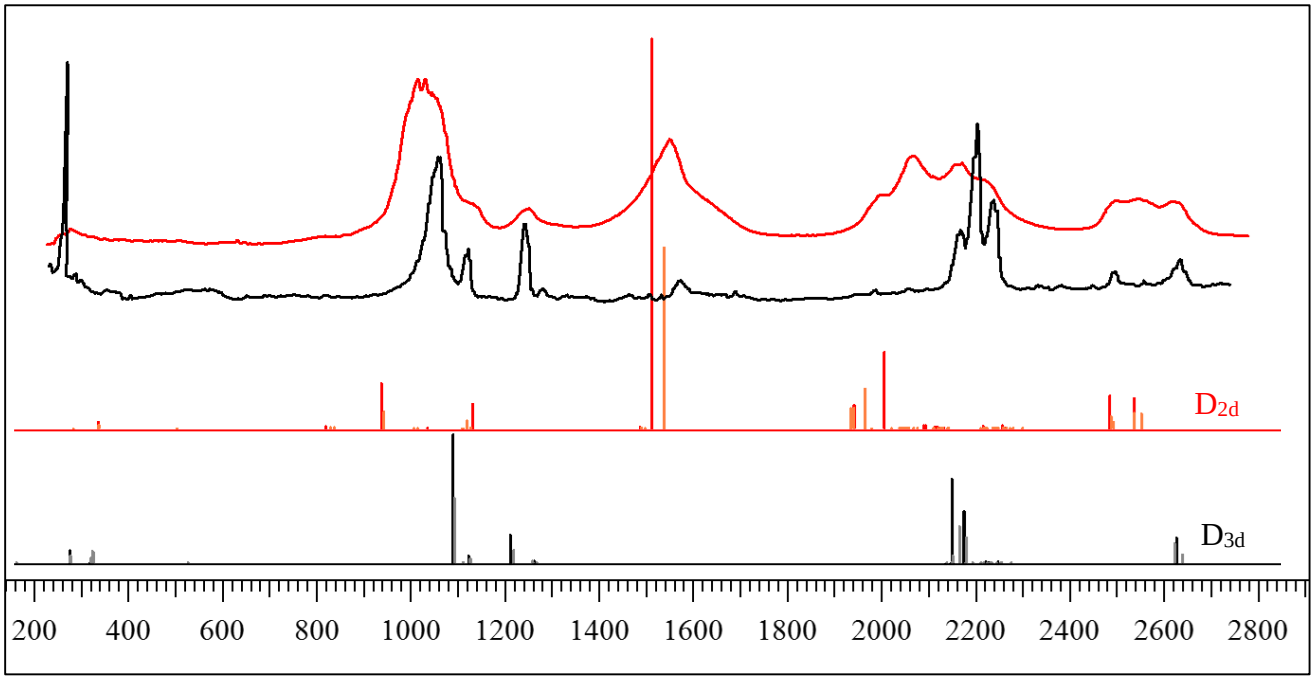

Fig 3.1: Vapor spectrum at room temperature (red), the matrix isolated spectrum (black), and the predicted anharmonic frequencies of D_{2d} (red sticks) and D_{3d} (black sticks) forms. The orange and gray sticks are for the D_{2d} and D_{3d} ^{11}B ^{10}B isotopomers respectively

The matrix isolation spectrum reported[10] for $Be(BH_4)_2$ isolated (0.3%) in solid argon at 20 K, shown as the black trace in Fig 3.1, is especially enlightening regarding the mixture. Nearly all the features attributable to the D_{2d} form are absent and only strong features near the positions predicted for the D_{3d} structure remain. There seems little doubt that the lowest energy form of $Be(BH_4)_2$ is that of the triply-bridged D_{3d} structure and that the barrier to interconversion is low enough that, at room temperature, significant populations exist for both D_{3d} and D_{2d} structures.

A comparison of observed and calculated gas phase intensities can give some measure of the relative amounts of the two forms of $Be(BH_4)_2$ at room temperature. The most intense feature predicted for the D_{2d} structure is the vibrational mode at 1511 cm^{-1}, with anharmonic intensity of 788 (km/mol) while the strongest D_{3d} transition occurs at 1089.3 with a predicted anharmonic intensity of 270 (km/mol). For a 50:50 mix of the two forms, the former D_{2d} band

would thus be about 3 times more intense than the latter D_{3d} feature. Instead this ratio is estimated to be about 0.7, suggesting a D_{2d}/D_{3d} ratio of about 0.25. A similar estimate from bands in the 1900 to 2300 cm^{-1} region gives a value of about 0.5. In both cases this is consistent with the conclusion from CCSD theory that the D_{3d} form is lower in energy. A simple calculation using the CCSD/CBS equilibrium energy difference (90 cm^{-1}) gives a D_{2d}/D_{3d} ratio of 0.39 but this is undoubtedly too high since, at room temperature, one should compute the free energy difference between the two forms ($\Delta G = RT \ln K$). Calculation of ΔG requires knowledge of the zero point energy and of the thermal distribution of energy at room temperature, however, this was not possible since the vibrational frequencies were not available for the CCSD(T)/CBS case.

Vibration-Rotation Spectra

When the vapor phase spectra were recorded in 1972[15], the best available resolution was about 0.25 cm^{-1} and no trace of any individual vibration-rotation transitions was resolved. Using the vibration-rotation parameters calculated in the present study (Tables 3.1-3.5), we have computed band contours for the four intense infrared fundamental occurring in the 1900-2300 cm^{-1} bridge stretching region (Fig. 3.2). These consist of one parallel (red) and one perpendicular (blue) band for each of the D_{2d} and D_{3d} structures. To more closely match the observed spectra, the band origins of these were variously increased by 15 to 50 $cm^{-1.}$ Also included in these simulations are the contours calculated for the $^{11}B^{10}B$ isotopomer of $Be(BH_4)_2$. (The relative abundances are $^{11}B^{11}B$ (64 %) , $^{11}B^{10}B$ (32 %), $^{10}B^{10}B$ (4%)). The band origins for the $^{11}B^{10}B$ isotopomers were determined from ab initio frequency shifts. The positions are generally about 3- 15 cm^{-1} higher than those of the $^{11}B^{11}B$ form except for the case of the lower frequency band where the $^{11}B^{10}B$ isotopomer shifts to lower frequency due to Fermi resonance.

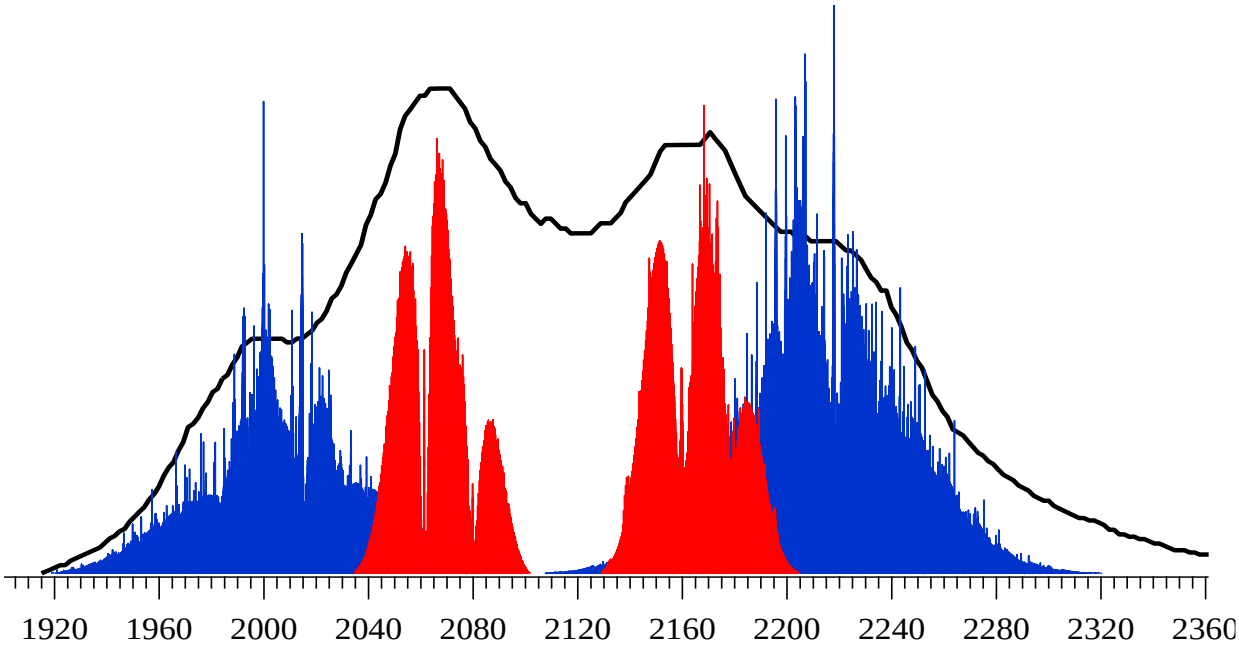

Fig. 3.2: 1920-2320 cm^{-1} region from room temperature spectrum (black trace) with the rotational bands contours in that region. Perpendicular (blue) and parallel (red) bands of D_{2d} on the left and D_{3d} on the right

The match of the band contours to the observed spectra is quite reasonable and the simulations predict that individual vibration-rotation transitions should be easily resolved. However, the spectra showed no such substructure at 0.25 cm^{-1} resolution or, surprisingly, even in later room temperature measurements by Al-Kahtani[17] and by Williams[26] using a 6-m FTIR instrument at the Pacific Northwest National Laboratory at 0.0015 cm^{-1} resolution. At 293 K, the Doppler width calculated for $Be(BH_4)_2$ is 0.002 cm^{-1} and collisional widths at the low pressures of the measurements should be comparable. Thus the most likely explanation for the absence of resolved features is believed not to be due to line broadening but rather to spectral congestion. Possible causes of this are considered below.

Causes of Spectral Congestion

Congestion in the spectra of $Be(BH_4)_2$ could arise from several sources. The first of these could be overlapping transitions of the D_{3d} and D_{2d} forms of the molecule since they both

exist with fairly small difference in energy. The second is the presence of the three isotopic forms for each structure. A third cause would be the overtone and combination transitions from the ground state; as seen in Tables 3.3 and 3.5, in the bridge stretching region, the intensities of these are generally small but can be nonzero, especially if any of the levels is Fermi resonant with a level corresponding to the upper state of an intense infrared fundamental band.

Other major contributors to congestion in an infrared spectrum are transitions from low-lying vibrational states (hot bands) that have appreciable thermal population at room temperature. Such bands are commonly observed with small shifts from the associated fundamental transition, and with a relative intensity that is well-approximated by the Boltzmann factor for the lower level. The importance of these states can be seen in Table 3.6. The theoretical energies of Tables 3.1 and 3.3 were used to calculate the relative populations which are shown explicitly in Table 3.4 for levels below 500 cm^{-1} for both D_{2d} and D_{3d} forms of $Be(^{10}BH_4)_2$. Remarkably, less than 20% of the D_{3d} molecules exist in the ground state and this will be reduced again by a factor of 0.64 due to the distribution of isotopic forms. Moreover, thermal population of the D_{2d} levels will further reduce the absolute population of the D_{3d} ground state.

All of the above factors can contribute to spectral congestion but the contributions of the D_{2d} form and of all hot bands can be reduced if one lowers the sample temperature. This is not practical for a gas cell experiment because the sample will all condense at temperatures much below 0 C. However, low temperatures can be achieved in free jet expansions and an experiment of this type is described below.

Table 3.6: Population of low frequency modes (below 500 cm^{-1}) at room temperature 298 K

D_{2d}		Freq.	Population	
Mode	degeneracy	(anharm)	ratio	percentage%
ν_{20}	2	121.2	1.11	18.5
$2\nu_{20}$	3	254.9	0.88	14.7
$3\nu_{20}$	2	363.6	0.35	5.8
$4\nu_{20}$	5	484.8	0.48	8.0
ν_8	1	286.0	0.25	4.2
ν_{19}	2	335.9	0.4	6.7
$\nu_{20}+\nu_8$	2	403.9	0.29	4.8
$\nu_{20}+\nu_{19}$	2	442.7	0.24	4.0
$\nu_{20}+\nu_{19}$	2	457.9	0.22	3.7
ν_5	1	493.9	0.09	1.5
higher levels			0.69	11.5
ground state			1	16.7
Sum			6.00	100
D_{3d}				
ν_5	1	195.5	0.39	7.4
ν_{18}	2	275.4	0.53	10.1
$2\nu_5$	1	305.6	0.23	4.4
ν_{17}	2	318.7	0.43	8.2
ν_{13}	2	415.2	0.27	5.1
$\nu_{18}+\nu_5$	2	439.7	0.24	4.5
$\nu_{13}+\nu_5$	2	468.8	0.21	4
$\nu_{17}+\nu_5$	2	486.7	0.19	3.6
$\nu_{17}+\nu_{13}$	1	498.9	0.09	1.7
higher levels			1.68	32
ground state			1	19
Sum			5.25	100

Diode Laser Spectra of $Be(BH_4)_2$ cooled in a Jet Expansion

The diode laser experiment was carried out by Darren Williams using the expansion apparatus of Dr. Steve Sharp at the Pacific Northwest National Laboratory. This set up involved a slit jet expansion with multi-passing of a tunable infrared diode laser beam through the cooled sample. The expansion was a mild one, of about 1% $Be(BH_4)_2$ in argon. From other work with this apparatus, these conditions normally give little or no complexes with argon and produce translational and rotational cooling to 10 to 20 K. This cooling reduces the Doppler

width by about a factor of 4 and the low density eliminates collisional broadening so that the limiting resolution is close to that of the diode source, about 0.001 cm^{-1}.

Because of the limited amount and the hazardous nature of the sample, only one experiment was conducted, in the region of the bridge stretches near 2200 cm^{-1}, where power of the diode laser power was appreciable. Two narrow regions were examined, (2164-2167 cm^{-1}) and (2193-2197 cm^{-1}).[26] The first region occurs reasonably close to the ν_7 parallel mode of the D_{3d} structure, a fortuitous result since none of present theoretical results were available at the time of the experiment. A less fortuitous choice was the second region, which occurs in the region between the ν_7 parallel and ν_{14} perpendicular bands. These narrow segments of the spectrum can be seen in Figure 3.3, which displays vibration-rotation spectra calculated at 20 K for both bands, with the centers of these shifted to locations that best fit the room temperature spectra.

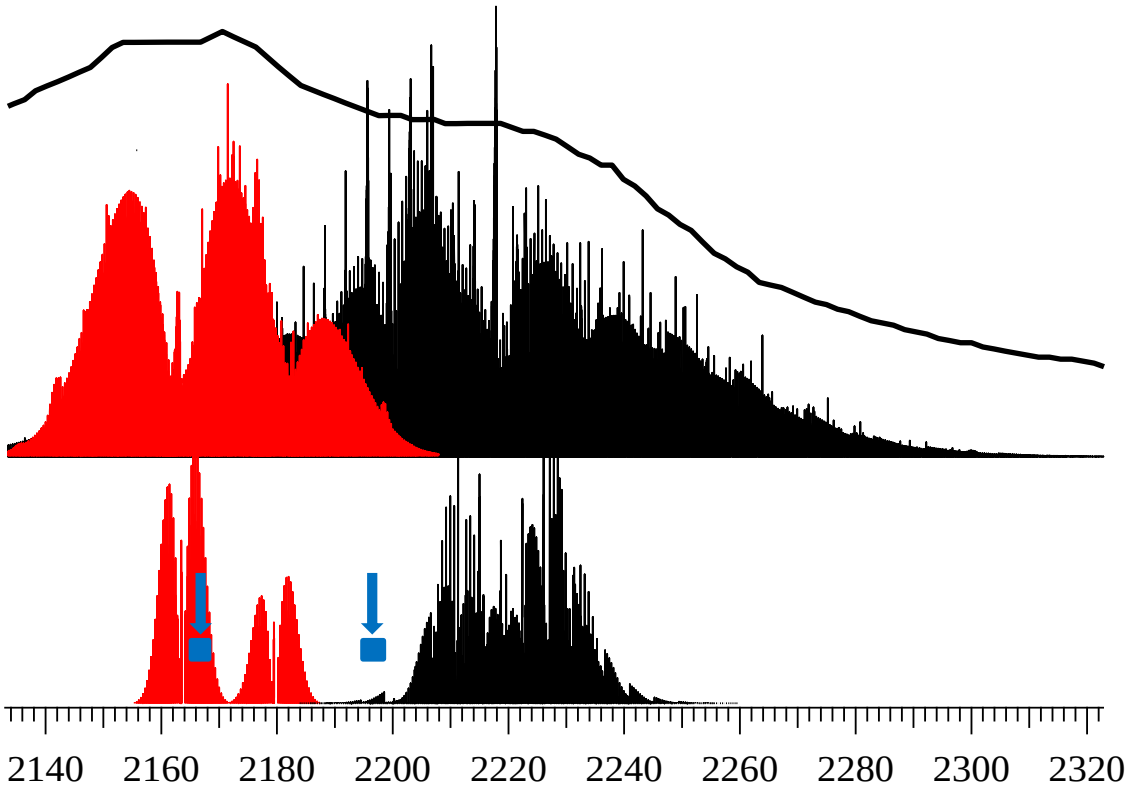

Fig. 3.3: Parallel and perpendicular bands of D_{3d} form at room temperature (up) and at 20 K (down). Blue boxes indicate the regions of the jet spectrum.

In the experiment, the infrared beam was split into three portions, with one sent through the sample, one sent through an etalon (to establish a linear scale), and the third through a N_2O reference gas cell (for absolute calibration). Details of the spectral processing are provided in the thesis of Williams.[26] The results for the region near 2165 cm^{-1} are shown in Figure 3.4 while the region near 2195 cm^{-1} is shown in Figure 3.5. In both cases, a high density of narrow vibration-rotation lines of about 0.002 cm^{-1} width are seen.

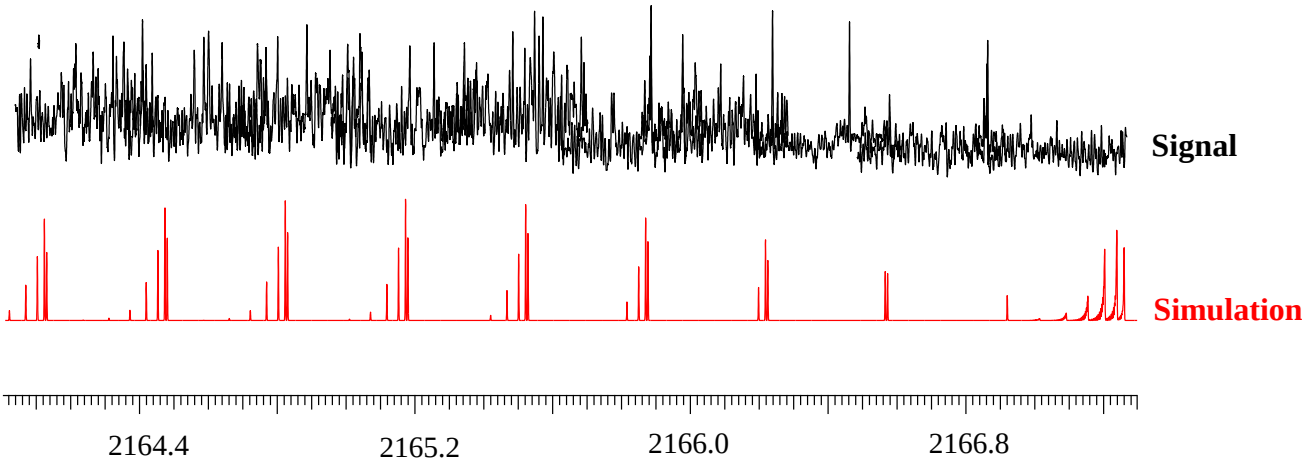

Fig. 3.4: The recorded spectrum at the region 2164-2167 cm^{-1} (black) and portion of the simulated parallel band (red).

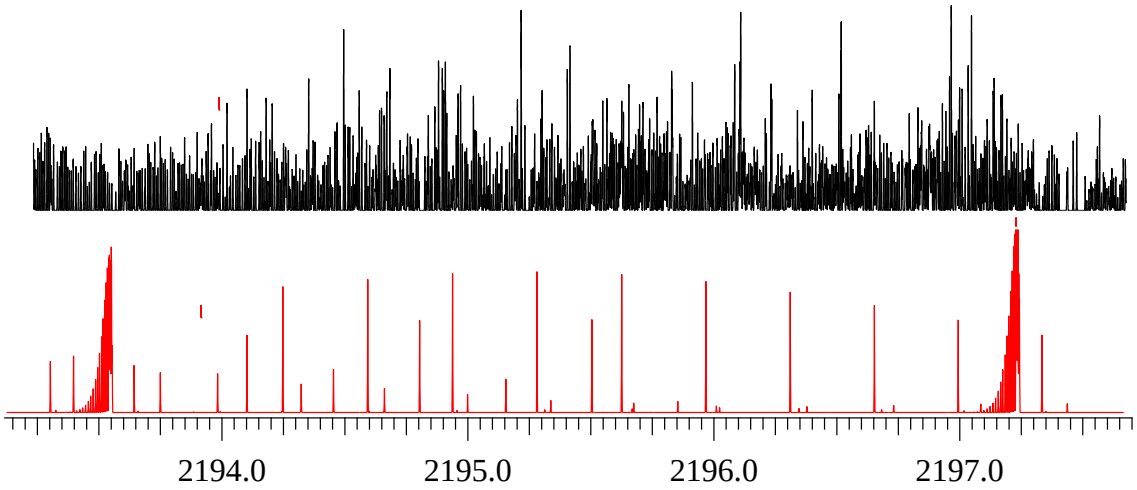

Fig. 3.5: The recorded spectrum in the region 2194-2197 cm^{-1} (black) and portion of the stimulated perpendicular band (red)

Figure 3.6A displays a portion of the 2195 cm^{-1} scan along with, at the bottom, a corresponding baseline obtained when the sample jet was turned off. The top trace in this spectrum shows this same region for an FTIR room temperature scan at 0.0015 cm^{-1} resolution; although the absorption is strong in this case, no features can be discerned due to congestion. The reproducibility of the measurements was quite good, as can be judged by the repeat scans shown in figure 3.6B. Full displays and a line listing of peaks in both spectral regions can be found in the thesis of Williams[26].

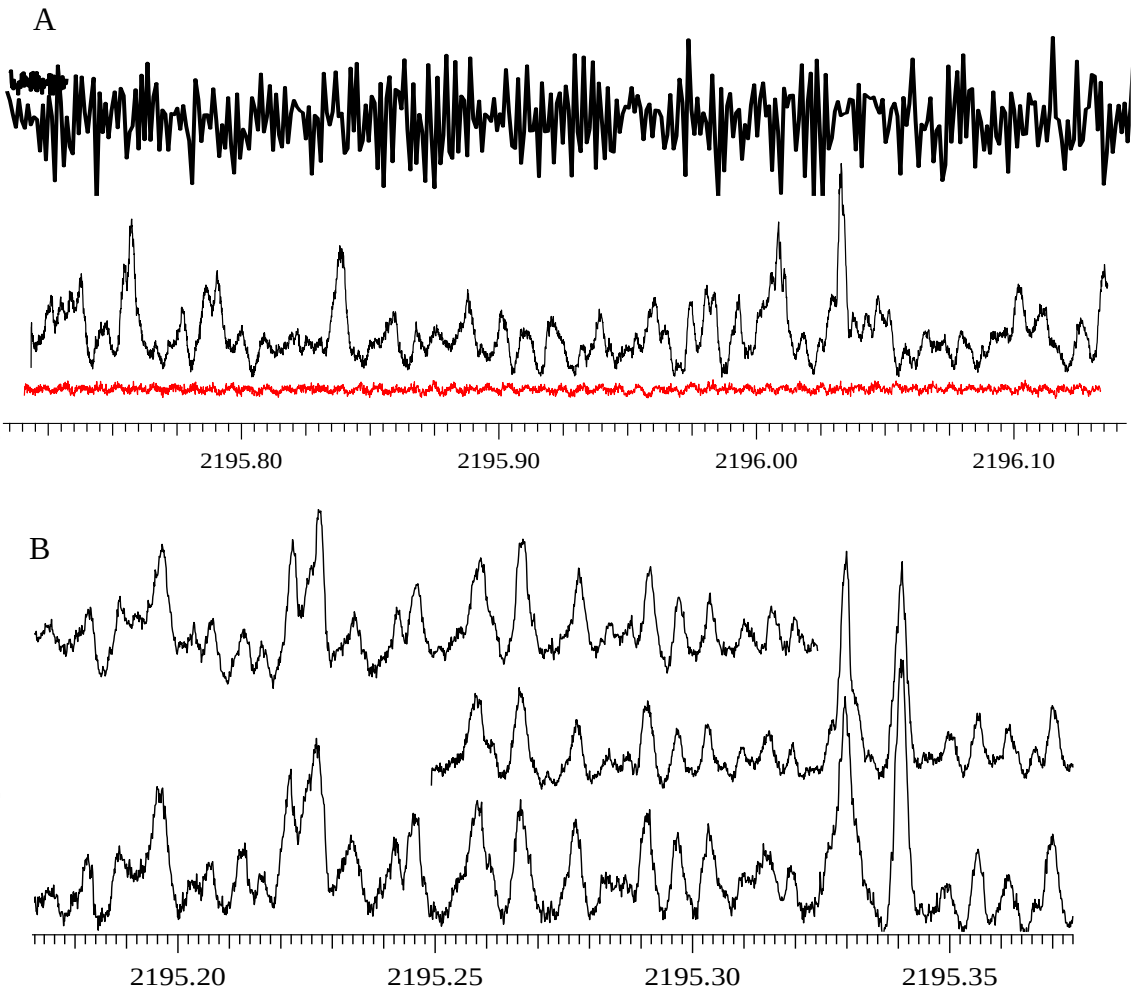

Fig. 3.6: A, Upper trace, FTIR spectrum at 0.0015 cm^{-1} resolution, lower traces, scan with sample on (black) and off (red). B, reproducibility of the peaks appeared by three scans of the same region

Using the theoretical parameters in tables 3.1-3.5, parallel and perpendicular spectra were generated for a 20 K temperature (Figure 3.3), with the hope of identifying spectral patterns in the jet spectra. In the 2165 cm^{-1} region, a parallel band is expected and a 3 cm^{-1} simulation is shown in Figure 3.4 that includes the Q branch and several low J R lines. Despite the cooling in the jet, the line density in the observed spectrum was more than 5 times that in the simulation. No clear match with experiment could be discerned as the simulation was moved along the wavenumber axis.

A similar result was found in the 2195 cm^{-1} region, where the simulation was of a perpendicular band. The experimental scans showed intriguing clusters of features resembling Q-branches (Fig. 3.7A, B) but efforts to simulate these using the predicted ν_{14} parameters showed no reasonable match. For example, the theoretical estimates predict shading to the low energy side for most Q branches ($\alpha = -\Delta B > 0$). Such shading is seen in 3.7A but the line spacings and intensities do not match well the simulations, nor are the associated P and R lines for such a Q branch identifiable. Similar problems occur for the case displayed in Fig 3.7B which looks like a Q branch shaded to the high energy side, something that is not predicted for any vibrational modes in this region.

Compared to a parallel band, the pattern of lines of a perpendicular band is less obvious and the line density is higher so that assignment of J, K values for a given feature was not possible. In both narrow segments of the experimental jet spectra, the observed density of lines was about 6 times higher than what would be expected for a single vibration-rotation band. Part of this higher density can be attributed to $^{10}B^{11}B$ and $^{11}B^{11}B$ isotopomers but the rest may be due to overtone-combination bands or to residual hot bands due to incomplete vibrational relaxation of the lower vibrational levels.

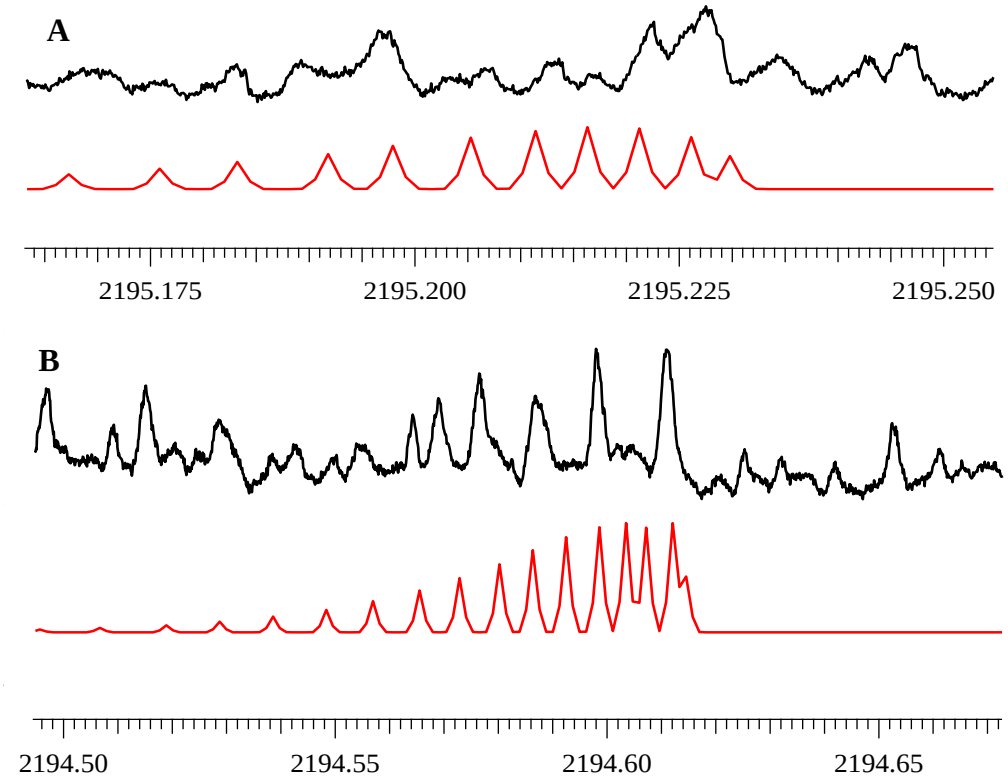

Fig. 3.7: A, comparison of computed Q branch (red) with cluster of lines in the spectrum (black). B, other cluster of lines resembles a backward Q branch (black) in the spacing between the lines.

Conclusions

The theoretical calculations presented in this thesis show that the potential energy surface of $Be(BH_4)_2$ has several local minima, with the lowest corresponding to D_{2d} and D_{3d} structures. The barrier between these is quite low (about 553 cm^{-1}) and the complete basis set prediction for the DFT calculations is that the D_{2d} structure has the lowest energy, with the D_{3d} form 97 cm^{-1} higher. The opposite ordering is obtained for the CBS limit from coupled cluster calculations, a result that is considered to be more reliable. Calculation of the harmonic and anharmonic frequencies gave zero point energies difference of about 200-250 cm^{-1}, in a direction that favors the D_{3d} structure as the low energy form.

The theoretical results also permitted reexamination of infrared spectra previously obtained for $Be(BH_4)_2$. The predicted anharmonic frequencies and intensities clearly show that the vapor at room temperature consists of an equilibrium mix of the two molecular forms, the D_{3d} form being dominant. Cooling of this sample to 20 K by isolation in argon gives a spectrum with D_{3d} features only, confirming the coupled cluster prediction.

Vibration-rotation parameters calculated at the anharmonic level permitted more reliable calculations of the band contours seen in room temperature spectra. Similar simulations of parallel and perpendicular bands at 20 K were calculated for comparison with diode laser jet spectra, which showed resolved transitions. However, due to the limited spectral range and high line density in these scans, it was not possible to discern patterns resembling the simulations. The high complexity of the jet spectra is likely due to congestion caused by contributions of ^{10}B, ^{11}B isotopomers, overtone and combination bands, and possibly hot bands for transitions originating from unrelaxed low vibrational states. In any future measurements of this type, it would be desirable to use only one isotopic form and to take spectra closer to the band origins, which we estimate to be 2220 cm^{-1} (ν_{14}) and 2163 cm^{-1} (ν_7). It might also be

good to use helium as a driving gas at higher pressures, to achieve a lower rotational, and perhaps vibrational, temperature.

Finally, the theoretical results obtained here show only one local minimum form of $Be(BH_4)_2$ that would be polar, and this "triangular form" is at high energy so the population density should be low. Thus one must question the previous report of a significant dipole moment in this molecule. In particular, the magnitude of the dipole was based on a dielectric result based on measurements in a cell with metal electrodes. Subsequent work has shown that $Be(BH4)_2$ can decompose on metal surfaces and this might have been enhanced since the dielectric cell was heated, due to the low volatility of $Be(BH4)_2$. Thus this measurement can be reasonably questioned. Harder to understand is the electric deflection result, which showed a clear deflection of a beam of $Be(BH4)_2$ in the quadrupolar deflection field. This could be due to trace amounts of the high energy triangular form or, since the beam was effusive with no vibrational cooling, could perhaps be due to an excited vibrational level with a nonzero value for the dipole moment.

Bibliography

[1]Burg, A. B., & Schlesinger, H. I. (1940). Metallo borohydrides. II. Beryllium borohydride. Journal of the American Chemical Society, 62(12), 3425-3429.

[2]Marynick, D. S., & Lipscomb, W. N. (1972). Crystal structure of beryllium borohydride. Inorganic Chemistry, 11(4), 820-823.

[3]Nibler, J. W., Shriver, D. F., & Cook, T. H. (1971). Infrared and Raman Spectra of Solid Beryllium Borohydride, BeB2H8. The Journal of Chemical Physics, 54(12), 5257-5266.

[4]Marynick, D. S. (1979). Model studies of the electronic structure of solid-state beryllium borohydride. Journal of the American Chemical Society, 101(23), 6876-6880.

[5]Gilliard Jr, R. J., Abraham, M. Y., Wang, Y., Wei, P., Xie, Y., Quillian, B. Robinson, G. H. (2012). Carbene-Stabilized Beryllium Borohydride. Journal of the American Chemical Society, 134(24), 9953-9955.

[6]Longuet-Higgins, H. C., & Bell, R. P. (1943). 64. The structure of the boron hydrides. Journal of the Chemical Society (Resumed), 250-255.

[7]Silbiger, G., & Bauer, S. H. (1946). The Structure of the Hydrides of Boron. VII. Beryllium Borohydride, BeB2H8. Journal of the American Chemical Society, 68(2), 312-315.

[8]Almenningen, A., Gundersen, G., & Haaland, A. (1967). On the molecular structure of beryllium borohydride. Chemical Communications (London), (11), 557-559.

[9]Morgan, G. L., & Cook, T. H. (1970). Infrared spectra and structure of beryllium borohydride. Journal of the American Chemical Society, 92(22), 6493-6498.

[10]Nibler, J. W., & Dyke, T. (1970). Electric deflection and dipole moment of beryllium borohydride. Journal of the American Chemical Society, 92(9), 2920-2922.

[11]Nibler, J. W., & McNabb, J. (1969). The dipole moment and infrared spectrum of beryllium borohydride. Journal of the Chemical Society D: Chemical Communications, (3), 134-135.

[12]Nibler, J. W. (1972). Infrared and Raman spectra of gaseoux and matrix isolated beryllium borohydride. Journal of the American Chemical Society, 94(10), 3349-3359.

[13]Gundersen, G., Hedberg, L., & Hedberg, K. (1973). Reinvestigation of the molecular structure of gaseous beryllium borohydride BeB2H8 by electron diffraction. The Journal of Chemical Physics, 59(7), 3777-3785.

[14]Brendhaugen, K., Haaland, A., & Novak, D. P. (1975). The gas phase electron diffraction pattern of beryllium borohydride.

[15]Nibler, J. W. (1972). Infrared and Raman spectra of gaseoux and matrix isolated beryllium borohydride. Journal of the American Chemical Society, 94(10), 3349-3359.

[16]Gaines, D. F., Walsh, J. L., & Hillenbrand, D. F. (1977). Gas-phase nuclear magnetic resonance spectroscopic study of the molecular structure of beryllium borohydride, Be (BH4)2. Journal of the Chemical Society, Chemical Communications, (7), 224-225.

[17]Al-Kahtani. A. A. PhD thesis, Oregon State University, 1995, High Resolution Spectroscopy of Metal Borohydrides.

[18]Armstrong, D. R., & Perkins, P. G. (1968). A theoretical study of beryllium borohydride BeB 2 H 8. Chemical Communications (London), (7), 352-354.

[19]Marynick, D. S., & Lipscomb, W. N. (1973). Ab initio self-consistent field and configuration interaction study of beryllium borohydride. Journal of the American Chemical Society, 95(22), 7244-7250.

[20]Ahlrichs, R. (1973). Structure of beryllium boron hydrides BeBH5and BeB2H8. Chemical Physics Letters, 19(2), 174-178.

[21]Ortiz, J. V., & Lipscomb, W. N. (1986, April). AB initio calculations on small boranes. In Boron-Rich Solids (Vol. 140, No. 1, pp. 274-287). AIP Publishing.

[22]Stanton, J. F., Lipscomb, W. N., & Bartlett, R. J. (1988). Structure, energetics, and vibrational spectra of beryllium borohydride isomers. The Journal of chemical physics, 88(9), 5726-5734.

[23]Bonaccorsi, R., Charkin, O. P., & Tomasi, J. (1991). Nonempirical study of the structure and stability of beryllium, magnesium, and calcium borohydrides. Inorganic Chemistry, 30(15), 2964-2969.

[24]Derecskei-Kovacs, A., & Marynick, D. S. (1994). The performance of a variety of density functional and ab initio methods on the structural problem of beryllium borohydride. Chemical physics letters, 228(1), 252-258.

[25]Saeh, J. C., & Stanton, J. F. (1997). Computational Evidence for a Metastable Polar Isomer of Beryllium Borohydride. Journal of the American Chemical Society, 119(31), 7390-7391.

[26]Williams, D. L. PhD thesis, Oregon State University (1997). High resolution infrared and Ab Initio studies of aluminum and beryllium borohydrides.

[27]Lewars, E. (2010). Computational chemistry: introduction to the theory and applications of molecular and quantum mechanics. Springer.

[28]Cramer, C. J. (2013). Essentials of computational chemistry: theories and models. John Wiley & Sons.

[29]Lowe, J. P. (2006). Quantum chemistry. Academic Press.

[30]Sherrill, C. D. (1995). An Introduction to Configuration Interaction Theory, 7-10

[31]Kümmel, H. G. (2003). A biography of the coupled cluster method. International Journal of Modern Physics B, 17(28), 5311-5325

[32]Cremer, D. (2012). From configuration interaction to coupled cluster theory: The quadratic configuration interaction approach. 14-15

[33]Helgaker, T., Jorgensen, P., & Olsen, J. (2013). Molecular electronic-structure theory. Wiley.

[34]Geerlings, P., De Proft, F., & Langenaeker, W. (2003). Conceptual density functional theory. Chemical reviews, 103(5), 1793-1874.

[35]Hohenberg, P., & Kohn, W. (1964). Inhomogeneous electron gas. Physical review, 136(3B), B864.

[36]Kohn, W., & Sham, L. J. (1965). Self-consistent equations including exchange and correlation effects. Physical Review, 140(4A), A1133.

[37]Levine, I. M. (2012). Quantum Chemistry7th ed, Pearson Boston MA.

[38]Peterson, K. A., Woon, D. E., & Dunning Jr, T. H. (1994). Benchmark calculations with correlated molecular wave functions. IV. The classical barrier height of the H+ H2→ H2+ H reaction. The Journal of chemical physics, 100(10), 7410-7415.

[39]Wilson Jr, E., Decius, J. C., & Cross, P. C. (1955). Molecular vibrations: The theory of infrared and Raman vibrational spectroscopy.

[40]Herzberg, G., & Spinks, J. W. T. (1966). Molecular spectra and molecular structure. Prentice-Hall.

[41]Allen, H. C., & Cross, P. C. (1963). Molecular Vib-rotors: The theory and interpretation of high resolution infrared spectra (Vol. 7). New York: Wiley.

[42]Sathyanarayana, D. N. (2007). Vibrational spectroscopy: theory and applications. New Age International.